CFD Letters

Journal homepage:
https://semarakilmu.com.my/journals/index.php/CFD_Letters/index
ISSN: 2180-1363

Thermo-Solutal Convection of Carreau-Yasuda Non-Newtonian Fluids in Inclined Square Cavities Under Dufour and Soret Impacts

Selma Lounis[1], Redha Rebhi[2,3], Noureddine Hadidi[1], Giulio Lorenzini[4,*], Younes Menni[5], Houari Ameur[5], Nor Azwadi Che Sidik[6]

[1] Department of Process Engineering and Environment, University of Medea, LME, Medea 26000, Algeria
[2] Department of Mechanical Engineering, Faculty of Technology, University of Medea, Medea 26000, Algeria
[3] LERM - Renewable Energy and Materials Laboratory, University of Medea, Medea 26000, Algeria
[4] Department of Engineering and Architecture, University of Parma, Parco Area delle Scienze, 181/A, Parma 43124, Italy
[5] Department of Technology, University Center Salhi Ahmed Naama (Ctr Univ Naama), P.O. Box 66, Naama 45000, Algeria
[6] Malaysia-Japan International Institute of Technology, Universiti Teknologi Malaysia, Jalan Sultan Yahya Petra, Kuala Lumpur, Malaysia

ARTICLE INFO

Article history:
Received 4 January 2022
Received in revised form 13 March 2022
Accepted 14 March 2022
Available online 31 March 2022

Keywords:
complex fluids; Rayleigh-Bénard thermosolutal convection; Carreau-Yasuda model; Soret number; Dufour number

ABSTRACT

The thermosolutal convection of non-Newtonian fluids under Soret and Dufour influences within an inclined square enclosure is explored. The active walls are subject to constant and uniform concentrations and temperatures. On the other hand, they are impermeable and adiabatic. A Carreau-Yasuda model is utilized to determine the fluid behavior. A special attention is paid to the impact of rheological parameters (n, a, E and s), the thermal Rayleigh number Ra_T, Dufour number, D_f, Soret number, S_r, Lewis number, Le, buoyancy ratio, N, and the inclination angel, γ. The numerical findings are represented in terms thermal fields, iso-concentration, and viscosity apparent contours, and the influence of certain parameters on the variation of stream function, Nusselt and Sherwood numbers, and apparent viscosity is also inspected. The findings suggest that the rise of the time constant parameter, E, causes an increase in thermal and mass exchange for various power-law indices, n. The decrease of the of ratio of infinite-to zero-shear-rate viscosities, s, and parameter, a, enhances the both thermal and mass transfers. The rise of the orientation angel γ from 0° to 90° yields an increase in thermal and mass transfer, but without a specific pattern in the different parameters studied.

1. Introduction

The thermosolutal natural convection through enclosures with complex fluids is highly utilized in engineering or environmental applications such as; astrophysics, oceanography, and processing of food, geophysics, petrochemical, etc. [1-4]. The natural phenomenon of double diffusive convection was well documented and well mastered in the books [5-7]. Many authors inspected this phenomenon for Newtonian fluids, but with less focus on thermosolutal convection in complex fluids.

* *Corresponding author.*
E-mail address: Giulio.lorenzini@unipr.it (Giulio Lorenzini)

https://doi.org/10.37934/cfdl.14.3.96118

Performing a literature review up to date, several works on double diffusive convection resume interesting results. In square and rectangular enclosures, we can mention the work of Ohta *et al.,* [8] for pseudo plastic fluids. Kim *et al.,* [9] and Turan *et al.,* [10] inspected the convection a square enclosure differentially heated from the vertical sides, while Pericleous [11] and Lamsaadi *et al.,* [12] considered a cavity isothermally heated from the vertical sides. Lamsaadi *et al.,* [12] performed a scaling analysis with a good agreement found with the computed findings and they derived a correlation for Nusselt number. Balmforth [13] study, the linear stability theory led to $Ra_{TC}^{sup} = \infty$, which meant that the system was unconditionally stable. These findings were the results of the unsuitability of the rheology model for very weak shear convective flow. Convective flow bifurcations from the rest state occurs at zero flow amplitude convection, therefore at zero shear-rate. Thus, any kind of bifurcation that occurs at zero shear-rate will not be detected by any power-law model that was suggested for high shear-rate. However, the results of the nonlinear model indicated the existence of a threshold for finite amplitude, and it was predicted numerically vs. the main parameters. The threshold of the subcritical convection could be physical as the flow at the onset of convection is of finite amplitude type. The study achieved by Benouared *et al.,* [14] and Alloui and Vasseur [15] for Carreau-Yasuda fluids in a vertical cavity showed an important impact of the rheological parameters on the velocity, temperature and apparent viscosity variations within the enclosure. For inclined porous cavities, Kefayati *et al.,* [16] reported that the increased Soret and Dufour parameters alter the thermal behavior of power-law fluids. Khechiba *et al.,* [17] observed for Carreau-Yasuda fluids an important impact of the rheological parameters on the convective thermal exchange and flow behavior. Moreover, a significant influence was observed for the rheological parameters on the threshold for the onset of subcritical convective flow and Hopf bifurcation. Krishna and Reddy [18] utilized the Carreau-Yasuda model to examine the convection of power-law fluids through stumpy permeable porous medium. Wu *et al.,* [19] examined the influence of rheological and physical parameters on the convection in a cylindrical enclosure. Khellaf and Lauriat [20] analyzed the impact of the apparent viscosity of a Carreau shear-thinning fluid on the onset of oscillatory flows. The inspection realized by Raisi [21] on the convection of a complex fluid in a cavity having a pair of baffles illustrated that the reduced flow index improves the natural convection within the enclosure. Shahmardan and Norouzi [22] reported in their study on the convection of a complex fluid in a duct with a cavity that the decreased flow behavior index yields an augmentation in the fully development length. The survey realized by Guha and Pradhan [23] on the thermal exchange for complex fluids on a horizontal plate claimed that the shear-thickening fluids have a significant thermal exchange against Newtonian and shear-thinning fluids. Kefayati [24] verified and proved the efficiency of the lattice Boltzmann method for solving the thermal exchange of molten polymers in cavities. For both square and rectangular cavities, Vinogradov *et al.,* [25] observed the same hydrodynamic behavior for Newtonian and shear-thickening fluids, despite the clear difference in the thermal exchange rate for these fluids. Ben Khalifa *et al.,* [26] reported that the onset of stationary convection of a dilatant fluid in cavities occurred at a critical Rayleigh number of zero. For a Carreau-Yasuda fluid, Kefayati and Tang [27] remarked a gradual decrease in the rate of thermal and mass exchange with augmented power-law index within cubic cavities. Bihiche *et al.,* [28] interested in the case of a horizontal rectangular enclosure. Other interesting works may be found in Refs. [29-31]. Lamsaadi *et al.,* [32] reported that for a very high Rayleigh number, the Carreau and power-law models provide almost similar findings.

This inspection focused on double-diffusive natural convection across an inclined square cavity filled with a Carreau-Yasuda fluid. Thermal and solutal boundary conditions of the Dirichlet type are set on the upper and bottom walls, while the other walls were assumed well insulated. An attempt is conducted to present further demonstration on the impact of different main parameters.

2. Mathematical Foundation

The active walls of the studied enclosure are subjected to uniform temperature and concentration conditions, while the other walls are considered adiabatic. The enclosure, as show in Figure 1.

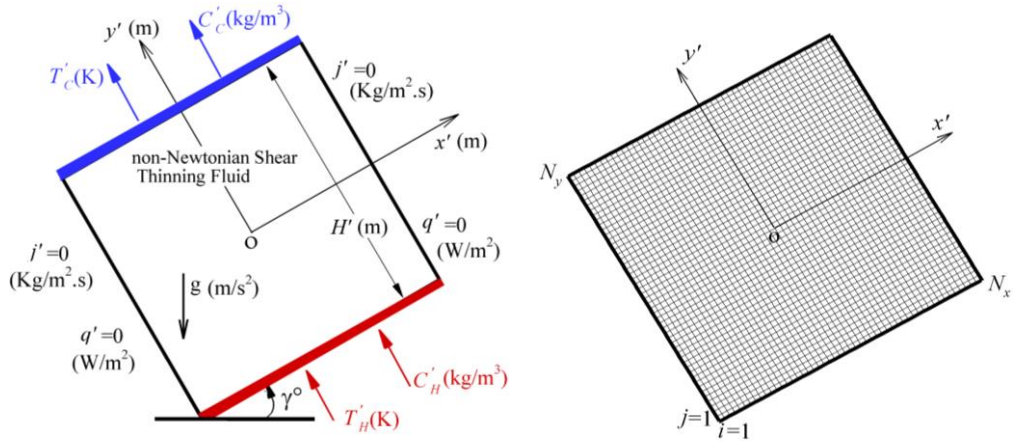

(a) (b)

Fig. 1. (a) Geometry of the physical problem; (b) Mesh generated.

The flow behavior is modeled using the Carreau-Yasuda model, where the fluid density, ρ, varies linearly with the temperature and solutal concentration as:

$$\rho = \rho_0\left[1-\beta_T(T'-T'_0)+\beta_C(C'-C'_0)\right] \tag{1}$$

where ρ_0 is the fluid mixture density at reference temperature T' and T'_0 and solute fraction, $C' = C'_0$ and, β_T and β_C are the thermal and concentration expansion coefficients, respectively. The subscript 0 refers to the reference condition at the origin of the coordinate system.

The governing equations are [33]:

$$\frac{\partial u'}{\partial x'}+\frac{\partial v'}{\partial y'}=0 \tag{2}$$

$$\rho_0\left[\frac{\partial u'}{\partial t'}+u'\frac{\partial u'}{\partial x'}+v'\frac{\partial v'}{\partial y'}\right]=-\frac{\partial P'}{\partial x'}+\frac{\partial \tau'_{xx}}{\partial x'}+\frac{\partial \tau'_{xy}}{\partial y'}-\rho_0 g\left[\beta_T(T'-T'_0)+\beta_C(C'-C'_0)\right]\cos\gamma \tag{3}$$

$$\rho_0\left[\frac{\partial v'}{\partial t'}+u'\frac{\partial v'}{\partial x'}+v'\frac{\partial v'}{\partial y'}\right]=-\frac{\partial P'}{\partial y'}+\frac{\partial \tau'_{xy}}{\partial x'}+\frac{\partial \tau'_{yy}}{\partial y'}-\rho_0 g\left[\beta_T(T'-T'_0)+\beta_C(C'-C'_0)\right]\sin\gamma \tag{4}$$

where:

$$\tau'_{xx}=2\mu\frac{\partial u'}{\partial x'},\ \tau'_{yy}=2\mu\frac{\partial v'}{\partial y'} \text{ and } \tau'_{xy}=\tau'_{yx}=\mu\left(\frac{\partial u'}{\partial y'}+\frac{\partial v'}{\partial x'}\right) \tag{4a}$$

$$\frac{\partial T'}{\partial t'}+u'\frac{\partial T'}{\partial x'}+v'\frac{\partial T'}{\partial y'}=\alpha\left(\frac{\partial^2 T'}{\partial x'^2}+\frac{\partial^2 T'}{\partial y'^2}\right)+D_{TS}\left(\frac{\partial^2 C'}{\partial x'^2}+\frac{\partial^2 C'}{\partial y'^2}\right) \tag{5}$$

$$\frac{\partial C'}{\partial t'}+u'\frac{\partial C'}{\partial x'}+v'\frac{\partial C'}{\partial y'}=D\left(\frac{\partial^2 C'}{\partial x'^2}+\frac{\partial^2 C'}{\partial y'^2}\right)+D_{ST}\left(\frac{\partial^2 T'}{\partial x'^2}+\frac{\partial^2 T'}{\partial y'^2}\right) \tag{6}$$

where u' and v' are the velocity components, P' is the pressure, t' is the time, μ is the fluid viscosity, τ_{ij} is the deviator stress tensor, g is the gravitational acceleration, and α and D are the thermal and solutal diffusivities, respectively. The properties D_{TC} and D_{ST} are respectively the Dufour and the Soret diffusion coefficients. Utilizing the Carreau-Yasuda model [34-37], the viscosity, μ, is varying as:

$$\frac{\mu-\mu_\infty}{\mu_0-\mu_\infty}=\left[1+(E'\dot{\gamma}')^a\right]^{(n-1)/a} \tag{7}$$

where μ_0 and μ_∞ are the fluid mixture viscosities at of the fluid at zero and infinity shear rates, respectively, E' is the time characteristic of the fluid, $\dot{\gamma}'$ is the second invariant of the shear rate tensor, a is a dimensionless parameter describing the transition region, and *n* (less than unity for the pseudo-plastic fluid) is the power-law exponent characterizing the shear-thinning regime (degree of shear-thinning). Typically, for shear-thinning fluids: $0.2<n<1$ and $0.1<E'<100s$.

The following scales were used:

$$(x,y)=\frac{(x',y')}{H'};\quad (u,v)=\frac{(u',v')H'}{\alpha};\quad t=\frac{t'\alpha}{H'^2};\quad \psi=\frac{\psi'}{\alpha};\Omega=\frac{\Omega' H'^2}{\alpha};P=\frac{P'}{P^*};\quad T=\frac{(T'-T_0')}{\Delta T^*};$$
$$C=\frac{(C'-C_0')}{\Delta C^*};\Delta T^*=\ T_H'-T_C';\Delta C^*=\ C_H'-C_C';\mu=\frac{\mu_{CY}}{\mu_0} \tag{8}$$

As noted, the dimension of the fluid layer has been utilized as a typical size in Rayleigh-Bénard convection. The governing equations that inform the method activeness are uttered in cost of vorticity, Ω, temperature, T, concentration, C and stream function, Ψ, are obtained as follows:

$$\frac{\partial \Omega}{\partial t}+\frac{\partial(u\Omega)}{\partial x}+\frac{\partial(v\Omega)}{\partial y}=\Pr\left[\mu\nabla^2\Omega+2\left(\frac{\partial\mu}{\partial x}\frac{\partial\Omega}{\partial x}+\frac{\partial\mu}{\partial y}\frac{\partial\Omega}{\partial y}\right)\right]+\Upsilon_\Omega \tag{9}$$

$$\frac{\partial T}{\partial t}+\frac{\partial\psi}{\partial y}\frac{\partial T}{\partial x}-\frac{\partial\psi}{\partial x}\frac{\partial T}{\partial y}=\nabla^2 T+D_f\nabla^2 C \tag{10}$$

$$\frac{\partial C}{\partial t}+\frac{\partial\psi}{\partial y}\frac{\partial C}{\partial x}-\frac{\partial\psi}{\partial x}\frac{\partial C}{\partial y}=Le^{-1}(\nabla^2 C+S_r\nabla^2 T) \tag{11}$$

and the vorticity, Ω, is characterized specified that:

$$\nabla^2\psi=-\Omega \tag{12}$$

The source term Y_Ω, in Eq. (9), is given by:

$$\Upsilon_\Omega=\Pr\left[\left(\frac{\partial^2\mu}{\partial x^2}-\frac{\partial^2\mu}{\partial y^2}-2\frac{\partial^2\mu}{\partial x\partial y}\right)\left(\frac{\partial u}{\partial y}+\frac{\partial v}{\partial x}\right)+Ra_T\left(\frac{\partial T}{\partial x}+\varphi\frac{\partial C}{\partial x}\right)\cos\gamma+\left(\frac{\partial T}{\partial y}+\varphi\frac{\partial C}{\partial y}\right)\sin\gamma\right] \tag{13}$$

The apparent viscosity, μ, namely:

$$\mu(\dot{\gamma}) = s + (1-s)\left[1+(E\dot{\gamma})^{a}\right]^{(n-1)/a} \tag{14}$$

$$\dot{\gamma} = \left[4\left(\frac{\partial^2\psi}{\partial x\partial y}\right)^2 + \left(\frac{\partial^2\psi}{\partial y^2} - \frac{\partial^2\psi}{\partial x^2}\right)^2\right]^{1/2} \tag{15}$$

The power law index, *n*, characterize the fluid behavior and $E = E'\alpha / H'^2$ is a dimensionless characteristic time of the fluid. The corresponding dimensionless thermal boundary conditions applied on the walls of the system are [38]:

$$u = v = 0 \text{ and } \psi = 0 \text{ at } x = \pm\frac{1}{2} \text{ and } y = \pm\frac{1}{2} \tag{16a}$$

while the thermal and solutal boundary conditions:

$$\frac{\partial T}{\partial x} = \frac{\partial C}{\partial x} = 0 \text{ at } x = \pm\frac{1}{2}; \text{ and } T = C = \pm\frac{1}{2} \text{ at } y = \pm\frac{1}{2} \tag{16b}$$

In Eqs. (9)-(13), one notice the presence of thermal Rayleigh number Ra_T, the Lewis number Le, the buoyancy ration N, the Prandtl number, Pr, and Dufour, D_f, and Soret, S_r, parameters they are expressed as:

$$Ra_T = \frac{g\beta_T \Delta T^* H'^3}{\alpha\nu};\ Le = \frac{\alpha}{D};\ N = \frac{\beta_S \Delta C^*}{\beta_T \Delta T^*};\ \mathrm{Pr} = \frac{\mu_0}{\rho_0\alpha};\ D_f = \frac{D_{ST}\mathrm{D}C^*}{a\mathrm{D}T^*};\ S_r = \frac{D_{TS}\mathrm{D}T^*}{D\mathrm{D}C^*} \tag{17}$$

The local and average Nusselt and Sherwood numbers (*Nu*, Nu_m) and (Sh, $\mathrm{Sh_m}$), respectively, are given as:

$$Nu = -\left.\frac{\partial T}{\partial y}\right|_{y=\pm 1/2} - D_f \left.\frac{\partial C}{\partial y}\right|_{y=\pm 1/2}, \qquad Nu_m = \int_{-1/2}^{1/2} Nu\,dx \tag{18}$$

$$Sh = -\left.\frac{\partial C}{\partial y}\right|_{y=\pm 1/2} - S_r \left.\frac{\partial T}{\partial y}\right|_{y=\pm 1/2}, \qquad Sh_m = \int_{-1/2}^{1/2} Sh\,dx \tag{19}$$

3. Computations

A second order finite difference method with a uniform grid size was utilized to solve the main equations. The discretized vorticity, energy and the concentration Eqs. (9-11) were solved using the alternative direction implicit method (ADI). The following convergence criterion was verified:

$$\frac{\sum i \sum j \left|\psi_{i,j}^{k+1} - \psi_{i,j}^{k}\right|}{\sum i \sum j \left|\psi_{i,j}^{k}\right|} \le 10^{-8} \tag{20}$$

In this study, uniform mesh size was used for both x and y direction show that the numerical values of Ψ_0, Nu, Nu_m, Sh, Sh_m and μ determined at the enclosure center. Preliminary tests showed the grid of 150×150 to be adequate to simulate accurately the convective and the reduced computational time. These results are presented in Table 1 has a value for different mesh size (50×50; 75×75; 100×100; 150×150; and 200×200).

Table 1
Grid sensitivity study for $Ra_T = 10^4$, $Pr = 10$, $e = 10$, $N = -0.5$, $n = 0.6$, $E = 0.1$, $s = 10^{-2}$, $a = 2$ and $S_r = D_f = 0$.

$N_x \times N_y$	50×50	75×75	100×100	150×150	200×200
ψ_0	13.712	13.530	13.596	14.326	14.320
Nu	3.761	3.535	3.584	3.819	3.816
Nu_m	2.878	2.771	2.821	2.952	2.955
Sh	9.637	7.917	8.105	9.111	9.106
Sh_m	6.394	5.722	5.854	6.378	6.375
μ	0.260	0.261	0.261	0.261	0.261

The numerical code was validation by comparing the present results against the experiment [39] and Plows [40] for a Newtonian fluid ($n = 1$), γ = 0°, $S_r = D_f = 0$, $N = 0$ and variation value of Ra_T**.** The results in Table 2 compare the averaged Rayleigh number values and a good agreement is remarked.

Table 2
Comparison of Rayleigh number for a high Prandtl number.

Ra_T	Experiment [39]	Plows [40]	Present study	Present study vs. Experiment [39]	Present study vs Plows [40]
2000	1.13	1.20	1.19	6.0%	0.8%
2500	…	1.46	1.33	…	9.3
3000	1.60	1.65	1.53	4.4	7.5
5000	2.03	2.09	2.07	1.9	0.9
6000	2.15	2.23	2.19	1.8	1.8
8000	2.35	2.43	2.39	1.6	1.6
10000	2.50	2.60	2.58	3.1	0.7
20000	2.93	3.09	3.01	2.6	2.6

4. Findings and Analysis

The results of thermosolutal convection occurring in an inclined square cavity for $Pr = 10$ are presented here. The findings are carried for different amounts of the Carreau-Yasuda parameters, namely, n, E, a, and s, Ra_T, Soret number, S_r, Dufour number, D_f, buoyancy ratio, N, Lewis number, Le, and inclined angel, γ. Numerical results are obtained in range of: $0.4 \leq n \leq 1$, $0 \leq E \leq 100$, $0 \leq s \leq 1$, $0.1 \leq a \leq 2$, $-0.6 \leq D_f \leq 0.6$, $-1 \leq S_r \leq 1$, $1 \leq Le \leq 50$, $-1 \leq N \leq 1$ and $0^\circ \leq \gamma \leq 90^\circ$.

Figure 2 presents the streamlines, isotherms, iso-concentration and viscosity apparent contours for $n = 0.4, 0.6,$ and 1. The decreased n yields intensifies the flow patterns and increases the thermal magnitudes and iso-concentration on the hot wall, which means an enhancement in the convection process. As well as the fluid velocity, the viscosity decreases with decreasing of power-law index considerably.

Figure 3 displays the flow patterns, ψ, isotherms, T, isoconcentration, S, and apparent viscosity, μ, contours for different time constant parameter, E, (1, 0.6 and 0). The flow patterns are considered

single-cell, filling the entire cavity. A certain value of the stream lines in the enclosure center shows that the increased parameter E enlarges the vortices.

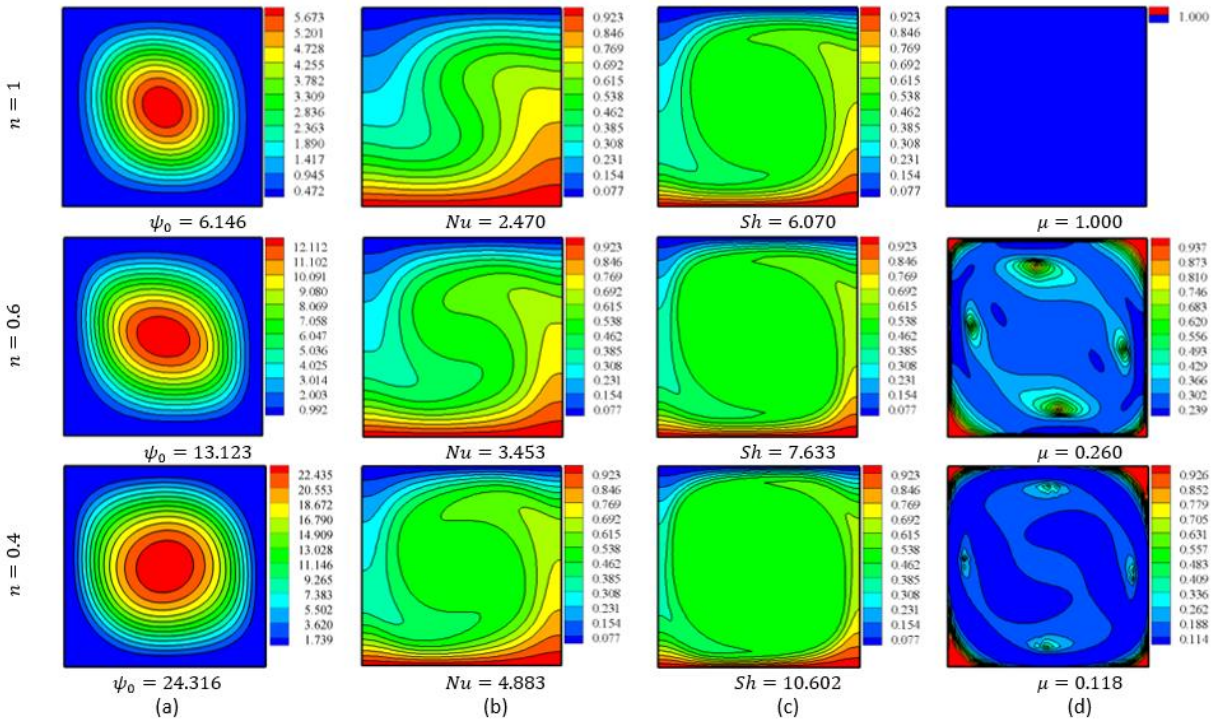

Fig. 2. Respective presentation of (a) streamlines; (b) isotherms; (c) is-concentration; (d) apparent viscosity, for $Ra_T = 10^4$, $Le = 10$, $N = -0.5$, $E = 0.1$, $a = 2$, $s = 10^{-2}$, and $\gamma = 0°$.

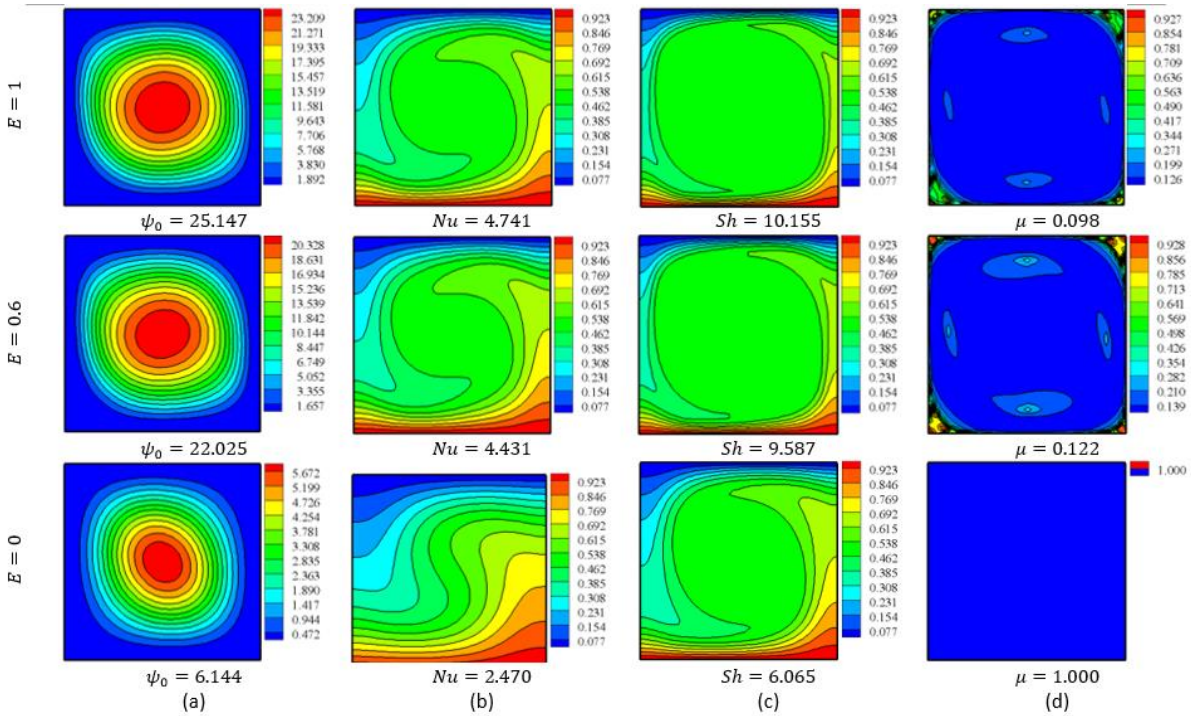

Fig. 3. Respective presentation of (a) streamlines; (b) isotherms; (c) is-concentration; (d) apparent viscosity, for $Ra_T = 10^4$, $Le = 10$, $N = -0.5$, $n = 0.6$, $a = 2$, $s = 10^{-2}$, $\gamma = 0°$ and different time constant parameter, E.

Moreover, the pattern is seen in the isotherms as they tilt toward the hot wall and their gradient increase slightly. The comparison between the iso-concentration demonstrates the rise of the

parameter E from 0 to 1 reason the gradient of the iso-concentration on the hot wall to increase considerably. This means an improved mass exchange due to the augmented E. As the parameter E increases, the viscosity decreases. In addition, the fluid becomes very viscous with decreased parameters E.

Figure 4 depicts the hydrodynamics, thermal fields, iso-concentration, and apparent viscosity. The flow patterns reveal an improvement in the convection process with decreased parameter s. In addition, the contours show that the density of iso-concentration on the hot wall increase with decreasing parameter s, which means an enhanced mass transfer. Furthermore, as the parameter s decreases, the apparent viscosity is reduced ($s = 1$, Newtonian fluid).

Figure 5 displays streamlines, isotherms, is concentration, and apparent viscosity in different values of parameter a. The motion of the streamlines confirms the model become the elliptical shape of the flow patterns change into a circular shape, which shows that the convection process increases considerably with decreasing parameter a. The contours show that the density of iso-concentration on the hot wall increase with decreasing parameter a. Hence, the patterns confirm that mass transfer improves with decreasing parameter a. In fact, the both thermal and solutal gradient on the hot wall is augment with the decreasing in parameter a, indication an increase in convective thermal and mass exchange rates. As the parameter a decrease, the apparent viscosity part fills almost the entire cavity, with the exception of a few small surrendered section near with walls. In fact, the viscosity is augment with parameter a decrease.

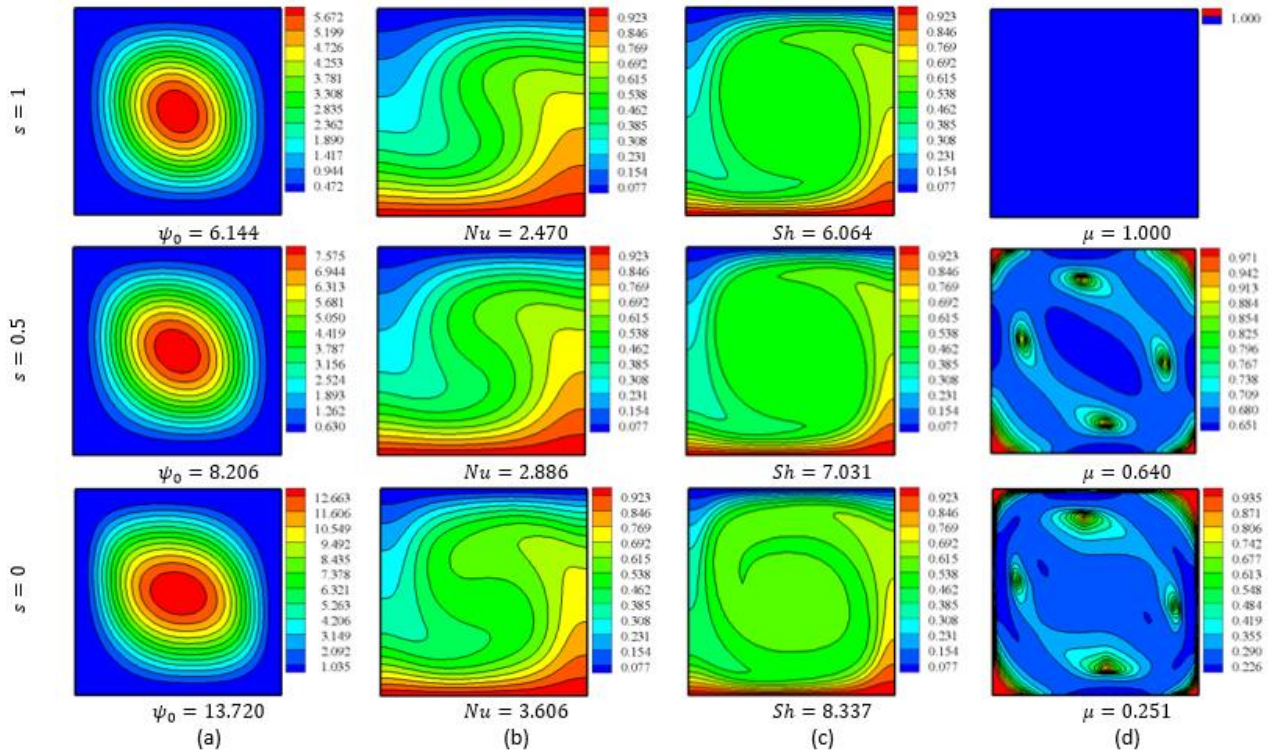

Fig. 4. Respective presentation of (a) streamlines; (b) isotherms; (c) is-concentration; (d) apparent viscosity, for $Ra_T = 10^4$, $Le = 10$, $N = -0.5$, $n = 0.6$, $a = 2$, $s = 10^{-2}$, $\gamma = 0°$ and different time constant parameter, E.

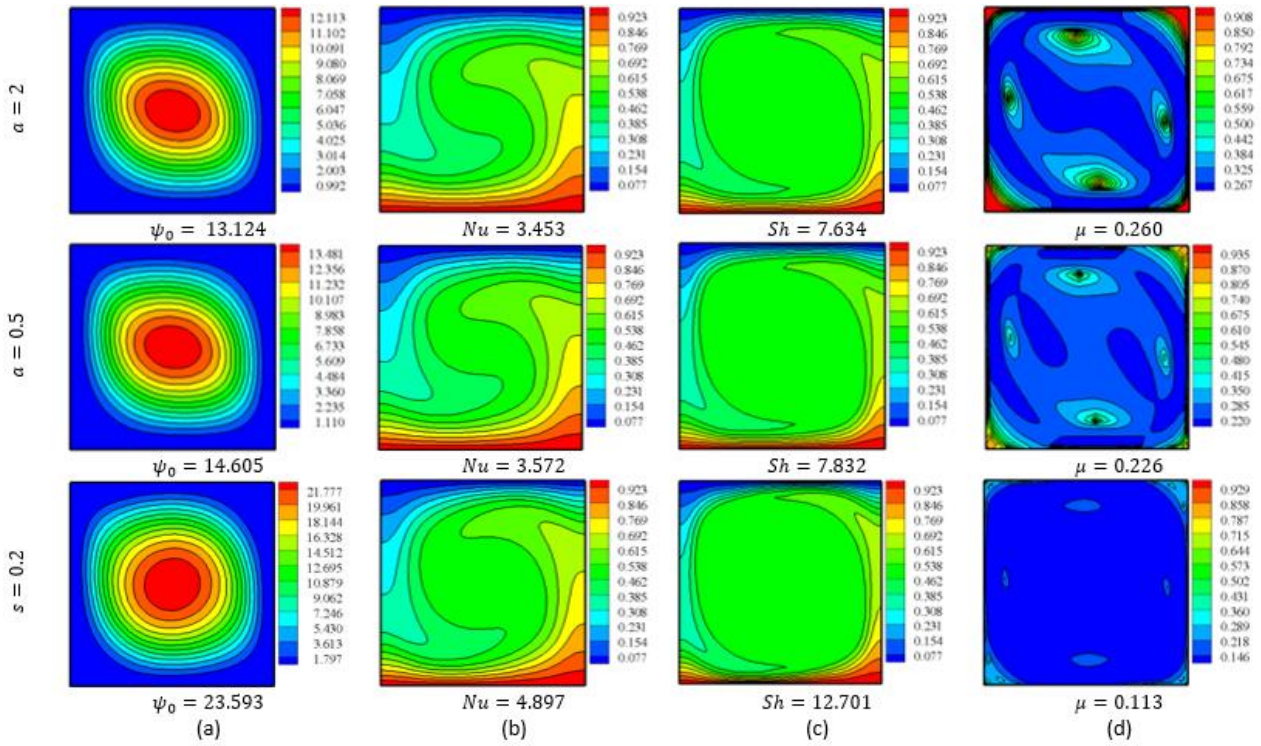

Fig. 5. Respective presentation of (a) streamlines; (b) isotherms; (c) is-concentration; (d) apparent viscosity, for $Ra_T = 10^4$, $Le = 10$, $N = -0.5$, $n = 0.6$, $E = 0.1$, $s = 10^{-2}$, $\gamma = 0°$ and different parameter, a.

Figure 6 displays the Soret number, S_r, effect on the streamlines, isotherms, is concentrations and viscosity apparent, contours. The streamlines do not vary noticeably with improved Soret number. The circulation of the thin core in flow patterns develops a little with the advancement of the Soret number. There is no significant alteration into isotherms with the component of the Soret number. While the Soret number is added to the concentration equation. The important effectuate of S_r observed in the isoconcentration gradient augment near the hot wall as the Soret number decrease from S_r = 0.6 to -0.6, which leads to the increase in convective mass transfer. No significant change in isotherms is noted. The site alteration of apparent viscosity is not significantly noted for different values of Soret number, this alteration is observed according to the parameter used in this mode.

Figure 7 resumes the Dufour effect, D_f, on the streamlines, thermal fields, is-concentrations and viscosity apparent contours. The flow is single-celled and fills the whole cavity; a cell rotation clockwise is observed. The specific vortex is enlarged and the gradient of isotherms is gradually augmented on the hot wall according to the augmented Dufour parameter. Also, an increase in the convection process and buoyancy force is observed due to the increase of the temperature. Moreover, the apparent viscosity increases with increased Dufour parameter from $D_f = -0.6$ to 0.6. However, no significant impact of Dufour parameter on iso-concentrations is observed, where the iso-concentrations move toward the hot wall slightly.

The profiles of apparent viscosity, μ, across the enclosure at mid-width location ($x = 0$) are plotted in Figures 8(a)-8(d) for $Ra_T = 10^4$, $Le = 10$, $N = -0.5$, $\gamma = 0°$ and $S_r = D_f = 0$. According to Eq. (14), it is seen that $\mu = 1$ when $n = 1, E = 0$ and $s = 1$, respectively. Upon decreasing the amounts of n and s or increasing those of E and a, the shear-thinning effect becomes considerable near the walls or at the cavity center, reducing thus the fluid viscosity and owing to high shear-rates.

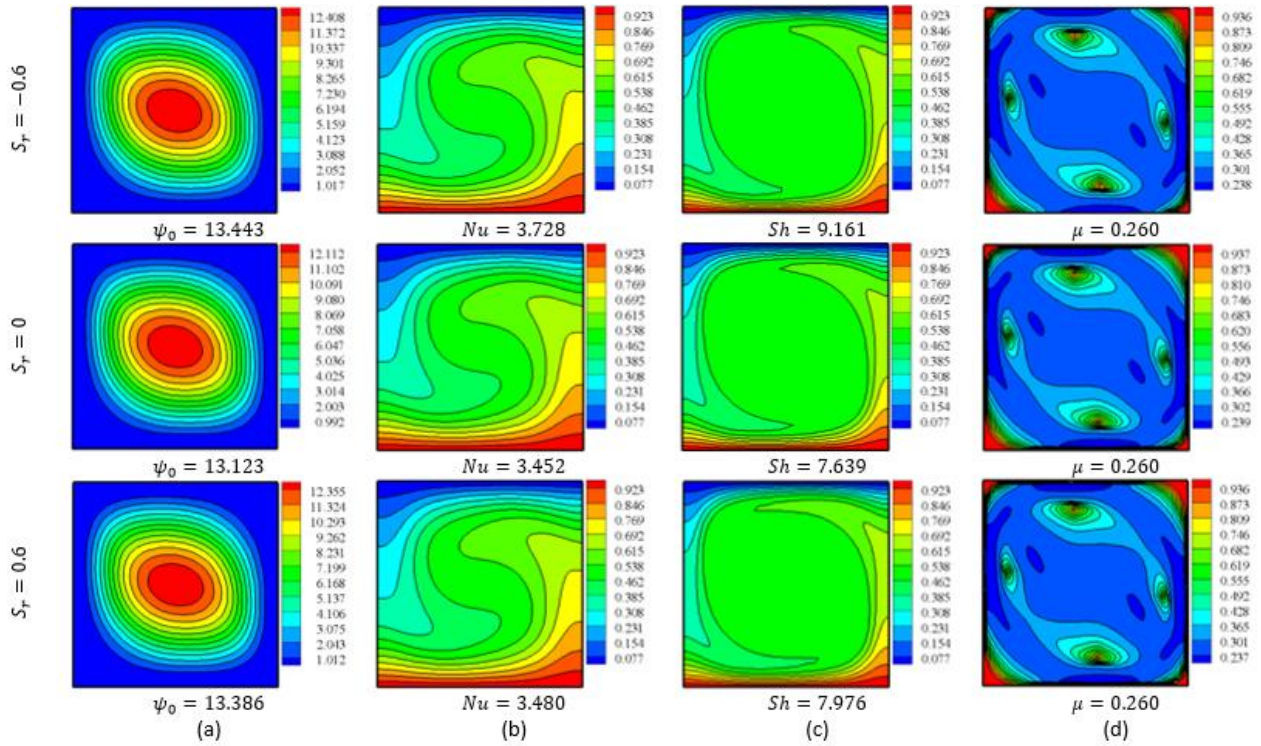

Fig. 6. Soret impacts on the (a) streamlines; (b) thermal fields; (c) iso-concentration; (d) viscosity apparent, for $Ra_T = 10^4$, $Le = 10$, $N = -0.5$, $n = 0.6$, $E = 0.1$, $a = 0$, $s = 10^{-2}$, $\gamma = 0°$ and $D_f = 0$.

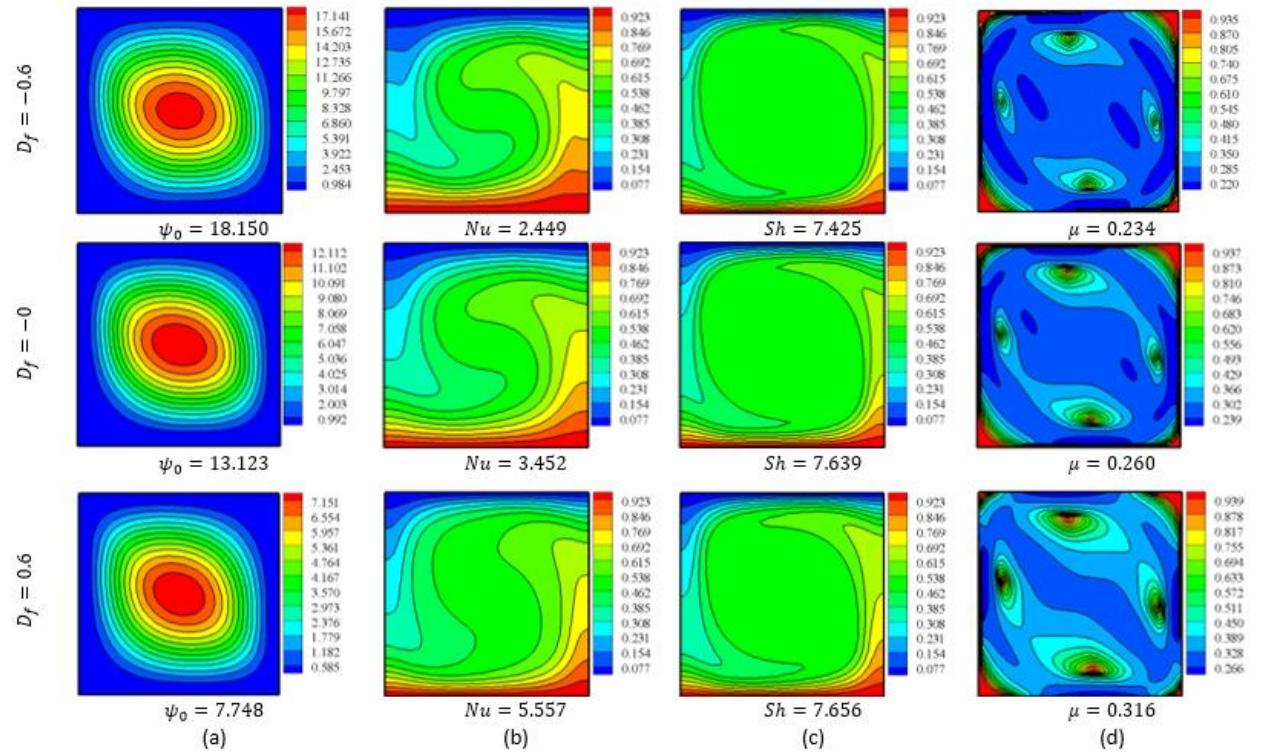

Fig. 7. Present the Dufour parameter effects, D_f, on (a) streamlines; (b) isotherms; (c) isoconcentration; (d) viscosity apparent, for $Ra_T = 10^4$, $Le = 10$, $N = -0.5$, $n = 0.6$, $E = 0.1$, $a = 0$, $s = 10^{-2}$, $\gamma = 0°$ and $S_r = 0$.

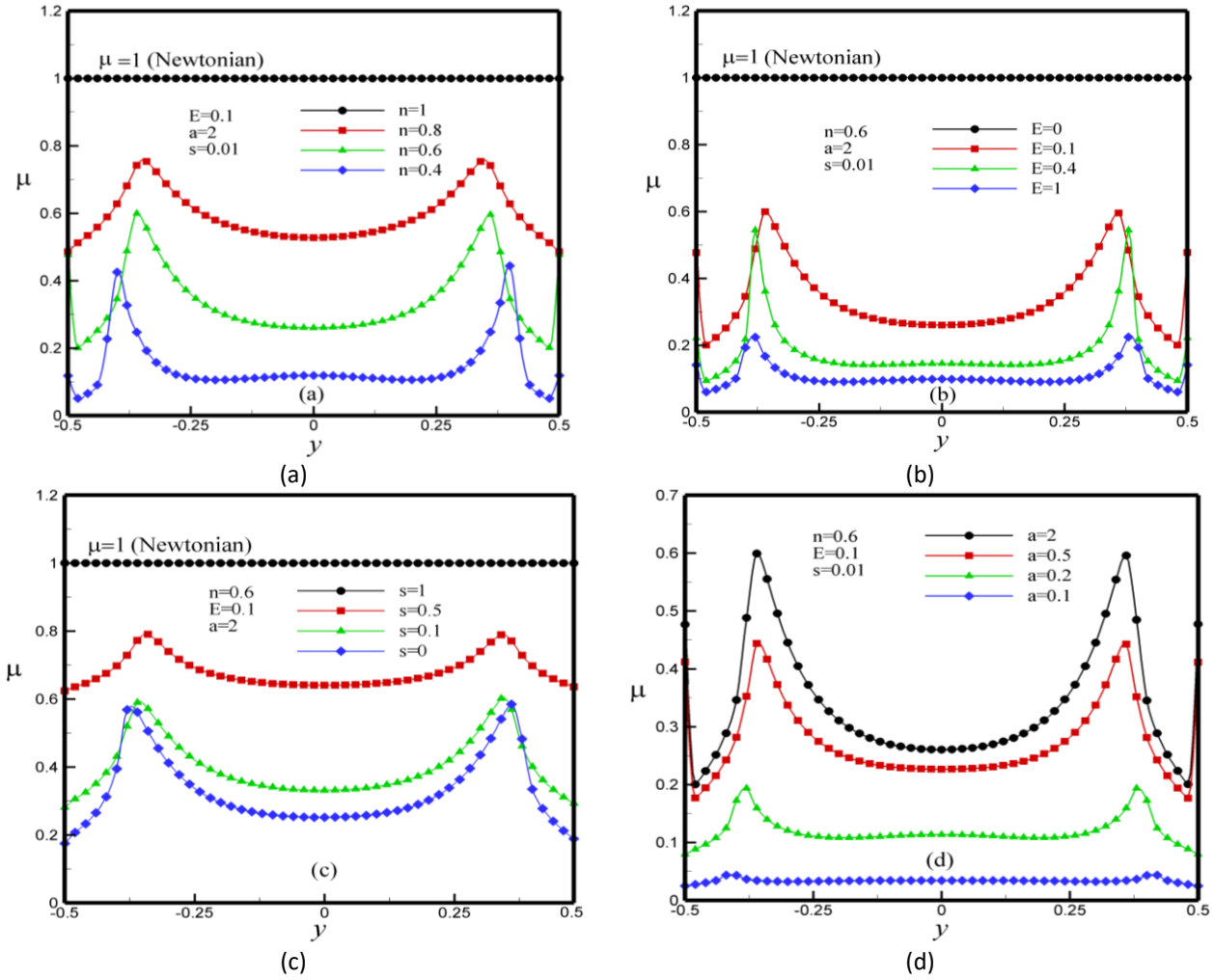

Fig. 8. Present the Apparent viscosity at $x = 0$: (a) influence of n; (b) influence of time constant parameter, E; (c) influence of s; (d) influence of parameter, a, for $Ra_T = 10^4$, $Le = 10$, $N = -0.5$, $\gamma = 0°$ and $S_r = D_f = 0$.

Comparing the results to a Newtonian case, the shear-thinning behavior is seen to enhance the convective circulation. This observation is identic to the findings claimed by Lamsaadi *et al.,* [12], Benouared *et al.,* [14] and Alloui and Vasseur [29] in their works on pure thermal convection in horizontal and vertical cavities.

Figure 9 shows the apparent viscosity versus shear rate. Figure 9(a) reveals an increase in the apparent viscosity with decreasing shear rate for different values of n. As shown by the computed results for $n = 1$, the apparent viscosity occurred at $\mu = 1$. From Figure 9(b), the increased parameter, E, induces a decrease in apparent viscosity. For $E = 0$, it was found that the apparent viscosity occurred at $\mu = 1$. Figure 9(c) shows that any increase of, s, yields an increase in apparent viscosity and $\mu = 1$ for $s = 1$. Figure 9(d) shows the effect of the parameter, a, on apparent viscosity. For a varying from 0.2 to 2, the apparent viscosity increases with increasing, a.

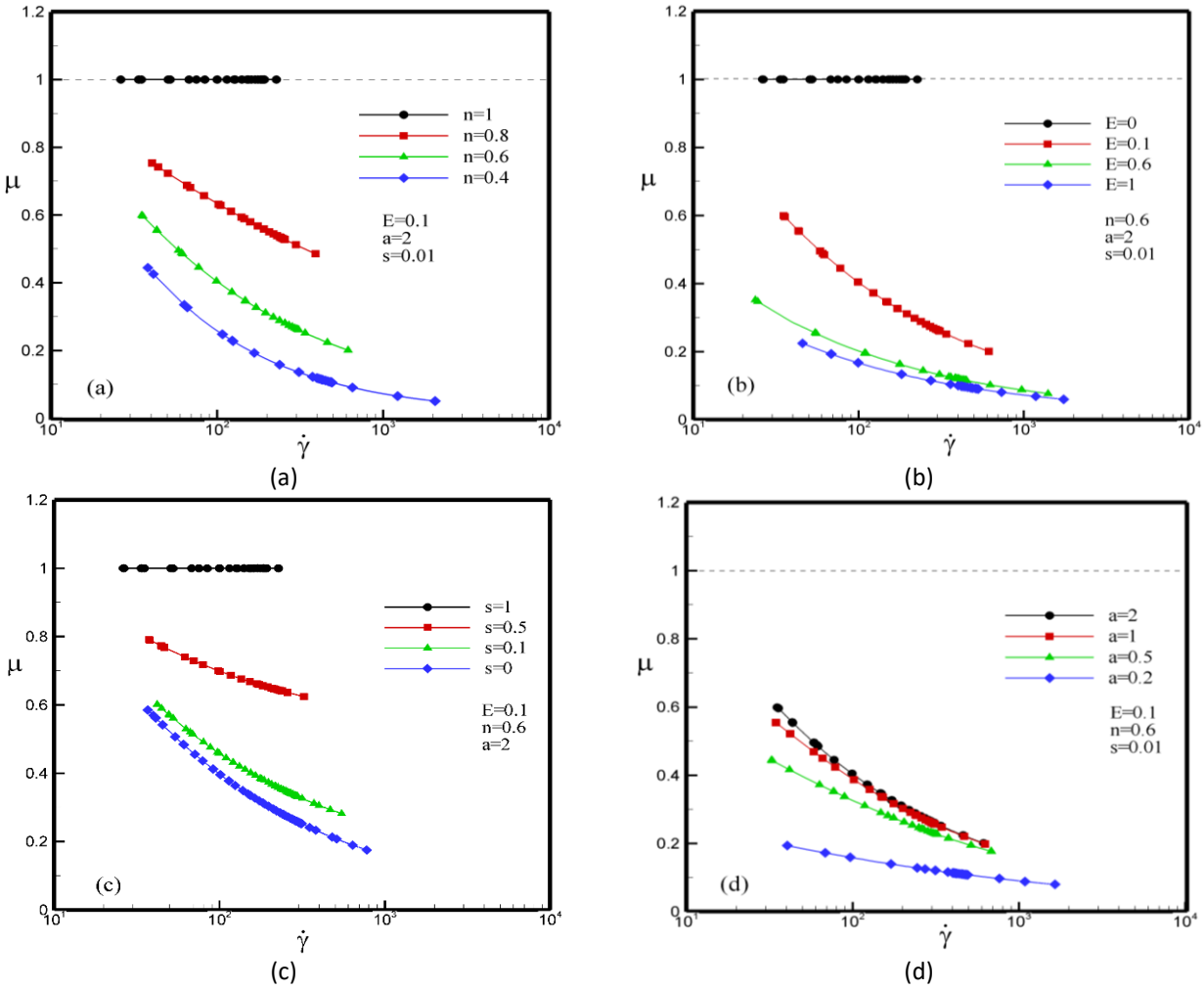

Fig. 9. Apparent viscosity, μ, vs. shear rate, $\dot{\gamma}$, for $Ra_T = 10^4$, $Le = 10$, $N = -0.5$, $\gamma = 0°$ and $S_r = D_f = 0$; impact of : (a) flow behavior index, n; (b) time constant parameter, E; (c) parameter, s; (c) parameter, a.

The impact of flow behavior index, n, on the stream function, ψ_0, apparent viscosity, μ, Nusselt number, Nu, and Sherwood numbers, Sh, vs. Ra for $Le = 10$, $N = -0.5$, $\gamma = 0°$ and $S_r = D_f = 0$ is presented in Figure 10. For $n = 0.4$ it is was found that both the stream function, the thermal and mass exchange rates, raised monotonically with augmented Rayleigh number Ra_T and that the apparent viscosity decreased shows in Figure 10(a)-(c). Figure 10(a) shows for $n = 0.4$ subcritical birufication is represented. The flow is defined by a passage from the rest state to a convection of delimited amplitude at $\psi_0 = 3.637$. This passage occurs at a subcritical Rayleigh number $Ra_{Tc}^{sub} = 2270$. Under the critical value, the result was purely conductive $\psi_0 = 0$, $Nu = Sh = 1$ and $\mu = 1$. Arises station at a Rayleigh of supercritical Ra_{TC}^{sup}, then the characterized regime is convective. For $n < 1$, the critical Rayleigh number (subcritical Rayleigh) is increased. For a given amount of Ra_T, the n value is decreased. In fact, that subcritical convection is highly influenced by the flow behavior index. In addition, the thermal and mass exchange rates are significantly enhanced. The apparent viscosity is significantly reduced with decreased n (Figure 10b).

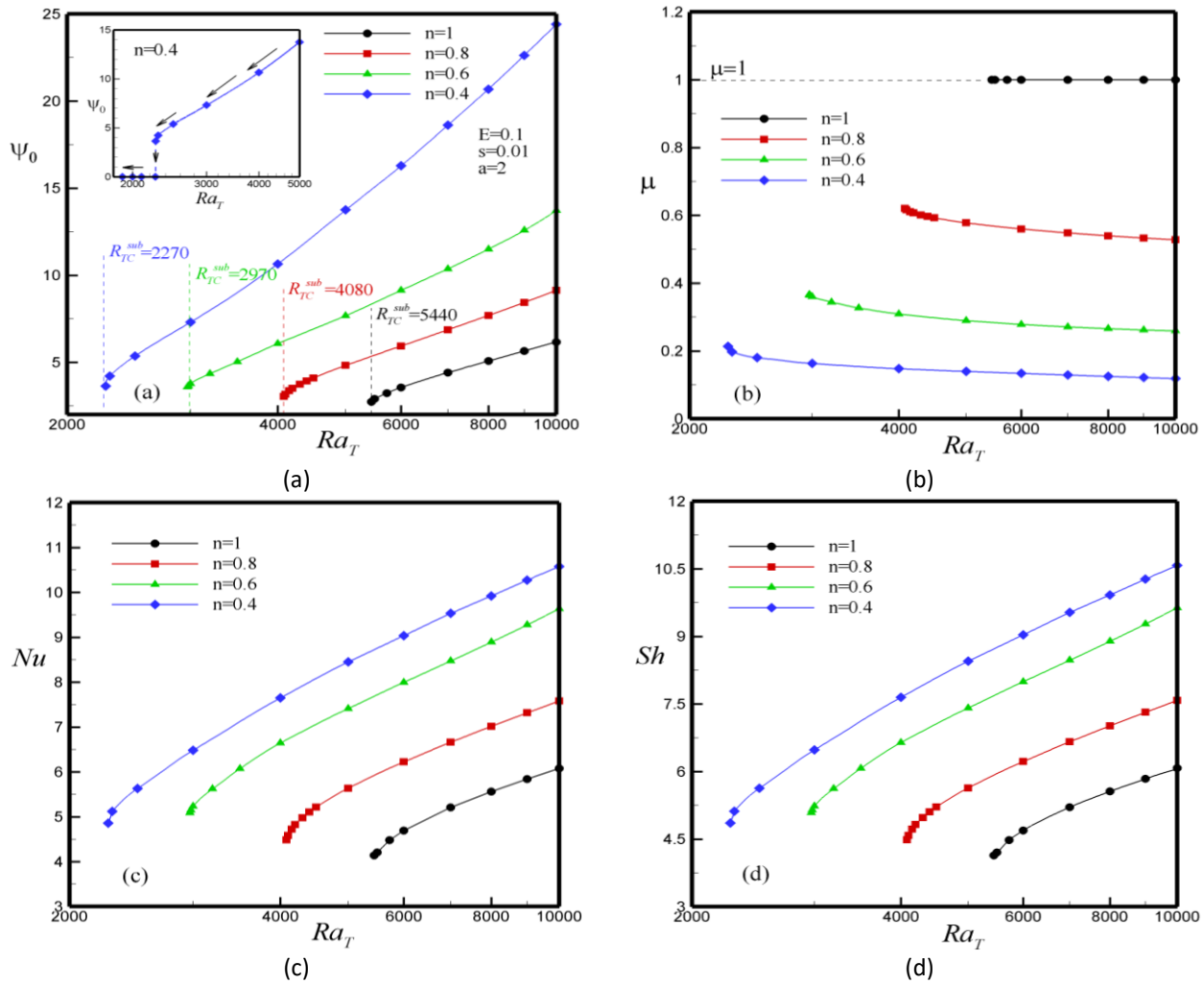

Fig. 10. Impact of Ra_T, n, on: (a) ψ_0; (b) apparent viscosity, μ; (c) Nu; and (d) Sh, for $Le = 10, N = -0.5, \gamma = 0°$ and $S_r = D_f = 0$.

Figure 11 displays the effects of parameter, a, on stream function, apparent viscosity, Nusselt number and Sherwood numbers as variations versus power-law index, n, at $Ra_T = 10^4$, $Le = 10$, $N = -0.5$, $E = 0.1$, $s = 10^{-2}$, $\gamma = 0°$ and $S_r = D_f = 0$. Where the decrease in parameter, a, the stream function increase presented in Figure 11(a). The stream function is small for $n = 1$ and increases with decreasing n. Figure 11(b) shows the changes in the apparent viscosity vs. the flow behavior index, n, for various amounts of the parameter, a, when the parameter, a , increase the apparent viscosity augment. Then we consider the influence of decreasing n on the decrease in apparent viscosity from top ($\mu = 1$) at Newtonian fluids to bottom at shear thinning fluids. From Figures 11c and 11d, Nu and Sh increase with the decreasing parameter, a. The convective thermal and mass exchange is improved by decreasing the parameter, a, while the behavior of Sherwood number becomes asymptotic. The apparent viscosity drops considerably as the parameter, a, decreases with decreasing n from 1 to 0. It is interesting to note that both Nu and Sh for Newtonian fluids are less and more than shear thinning fluids (pseudo-plastic $n < 1$).

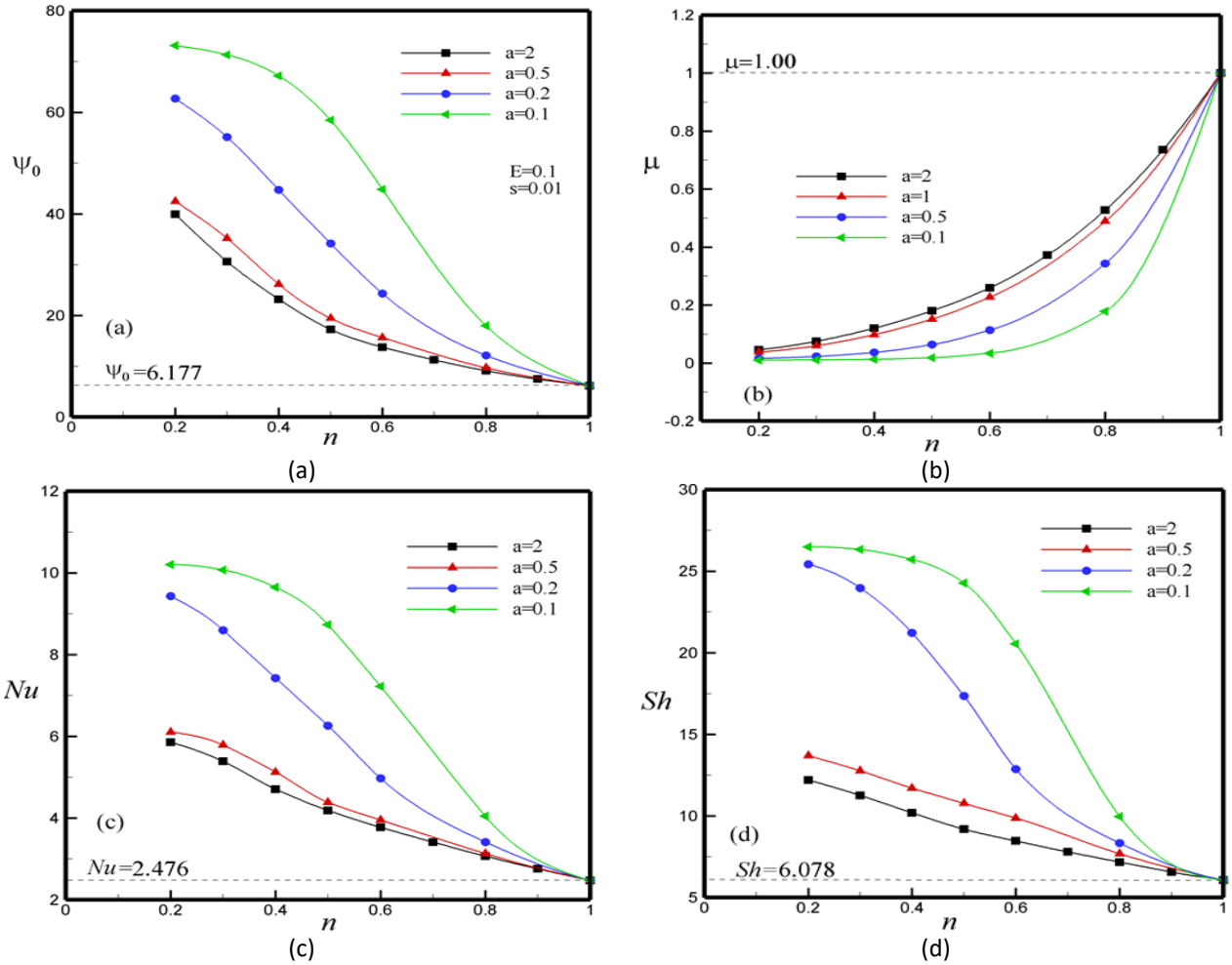

Fig. 11. Effect of parameter, a, and n, on: (a) stream function; (b) apparent viscosity, μ; (c) Nu; (d) Sh, for $Ra_T = 10^4$, $Le = 10$, $N = -0.5$, $E = 0.1$, $s = 10^{-2}$, $\gamma = 0°$ and $S_r = D_f = 0$.

Figure 12 displays the effect of time constant parameter, E, and flow behavior index, n, on stream function, apparent viscosity, Nusselt number and Sherwood numbers vs. n, at $Ra_T = 10^4$, $Le = 10$, $N = -0.5$, $a = 2$, $s = 10^{-2}$, $\gamma = 0°$ and $S_r = D_f = 0$. From Figure 12(a), the stream function changes and increases rapidly with augmented E at $\psi_0 = 6.177$. Figure 12(b) evaluates the influence of E on apparent viscosity, where it increases with decreased E. The apparent viscosity increases for various amounts of n, as the E parameter decreases. In addition, for $E = 0$ the apparent viscosity is close to 1, which confirms the Newtonian behavior. The results demonstrate also a considerable decrease in the apparent viscosity with decreasing, E, from 100 to 0. The apparent viscosity increases for shear thinning fluids (pseudo plastic fluids) ($n < 1$) and it decreases with increasing n. Furthermore, Nu and Sh increase with augmented E. So, the convection rates increase with the rise of E parameter. Figures 12(c) and 12(d) summarize the effect of n on Nu and Sh for different E. The thermal and mass exchange rates increase with increasing n, from 1 to 0.2. The drop of n augments Nu and Sh, which mentions that the decreased n enhances the thermal and mass exchange. Nu and Sh numbers are sensitive to the amounts of n and E. The augmentation in n and the decrease in E yield an important rise in the convection rates.

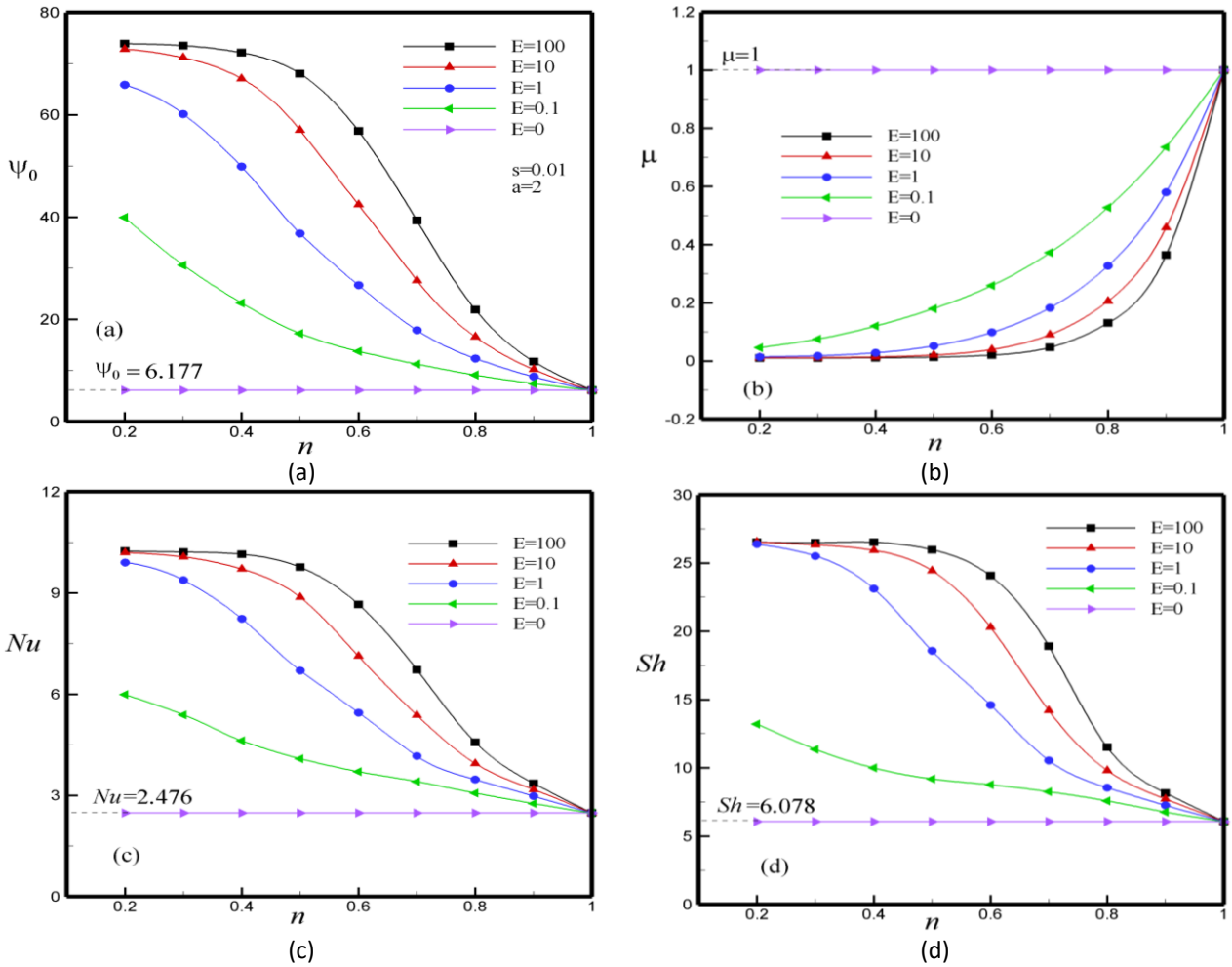

Fig. 12. Effect of time constant parameter, E, and n, on: (a) ψ_0; (b) μ; (c) Nu; (d) Sh, for $Ra_T = 10^4$, $Le = 10$, $N = -0.5$, $a = 2$, $s = 10^{-2}$, $\gamma = 0°$ and $S_r = D_f = 0$.

The influence of s and n on stream function, apparent viscosity, Nusselt number and Sherwood numbers for $Ra_T = 10^4$, $Le = 10$, $N = -0.5$, $E = 0.1$, $a = 2$, $\gamma = 0°$ and $S_r = D_f = 0$ shows in Figure 13. Figure 13(a) it shows that the stream function remains constant at $\psi_0 = 6.177$ for $s = 1$, then it increases gradually with decreased s. The stream function increases according to the decreased n. The apparent viscosity augments with the rise of s, reaching the top at $\mu = 1$ for $s = 1$. The viscosity decreases from top to bottom with n values for various amounts of s. Figures 13(c) and 13(d) exhibit the effect of the parameter s on Nu and Sh. The decreased s provokes an augmentation in Nu and Sh. Therefore, it proves that the convection rates rise with decreased s, which clearly shows the influence of n, demonstrating thus that the important enhanced convection with decreasing n (from Newtonian to shear-thinning fluids).

Figure 14 shows the effect of Dufour number, D_f, and n, on the stream function, apparent viscosity, *Nu* and *Sh* for $Ra_T = 10^4$, $Le = 10$, $N = -0.5$, $\gamma = 0°$ and $S_r = 0$. In Figure 14(a), the stream function increased with decreasing Dufour number, D_f, for $n < 1$. In addition, the stream function decreases with decreased D_f for $n = 1$. From Figure 14(b), the influence of D_f on the apparent viscosity is highlighted. The apparent viscosity increases with increased D_f. Also, the viscosity apparent is increased to the maximum value for $n = 1$.

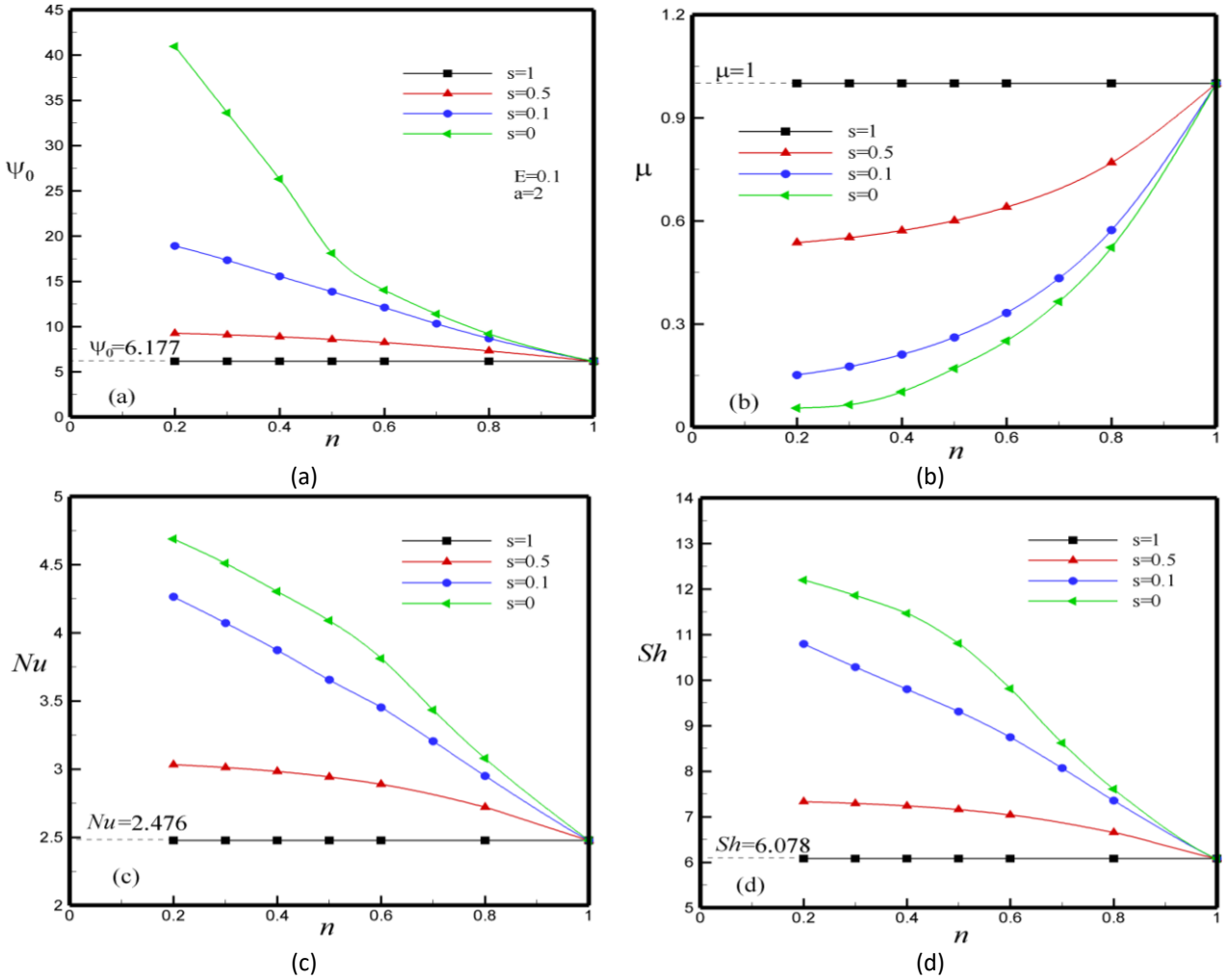

Fig. 13. Impact of s and n, on: (a) ψ_0; (b) apparent viscosity, μ; (c) Nu; (d) Sh, at $Ra_T = 10^4$, $Le = 10$, $N = -0.5$, $E = 0.1$, $a = 2$, $\gamma = 0°$ and $S_r = D_f = 0$.

However, for the small values of shear thinning fluids ($n < 1$), the viscosity is weak. Figures 14(c) and (d) show high *Nu* and *Sh* values with increasing D_f. As n, decreases, *Sh* increases with decreasing D_f. The mass transfer increases with decreasing n. It is observation to notation that the both Nu and Sh numbers for $n < 1$ are much than that of Newtonian fluids ($n = 1$).

The effect of Soret number S_r and n on the stream function, apparent viscosity, *Nu* and *Sh* is illustrated in Figure 15 at $Ra_T = 10^4$, $Le = 10$, $N = -0.5$, $\gamma = 0°$ and $D_f = 0$. From Figure 15(a), the stream function slightly increases with increased *Sr* from -1 to 1. For high values of n, ψ_0 gradually increases with decreasing n. In addition, the stream function increases with increased *Sr* for shear-thinnig fluids and it decreases with increased *Sr* for Newtonan fluids ($n = 1$). Figure 15(b) plots the apparent viscosity profile for different valeus of Soret number, whre no significant change is observed with decreased *Sr*. It is also observed that decreasing n from 1 to 0.4 decreases the apparent viscosity for all values of Soret number. Figures 15(c) and (d) resume the *Sr* influence on Nu and Sh. The increased *Sr* yields an increase in *Sh* and a small decline in Nu. Moreover, *Nu* and *Sh* increase with decreased n from 1 to 0.4. Also, the augementation in the thermal and mass exchange for shear-thining fluids is in contrary to the Newtonian fluids.

Figure 16 resumes the Le and *n* influence on the stream function, apparent viscosity, *Nu* and *Sh* for $Ra_T = 10^4$, $N = -0.5$, $\gamma = 0°$ and $S_r = D_f = 0$. When *Le* is increased from 1 to 50, the stream function increases. The decreasing n decreases the stream function for all values of Le. The effect of

Le on apparente viscosity is displayed in Figure 16(b), where the apparent viscosity increases slighthy with decreased Le. Decresing the value of n, the apparent viscosity decreases in a monotonic way until a constant value for shear-thinnig fluids, $n = 0.4$.

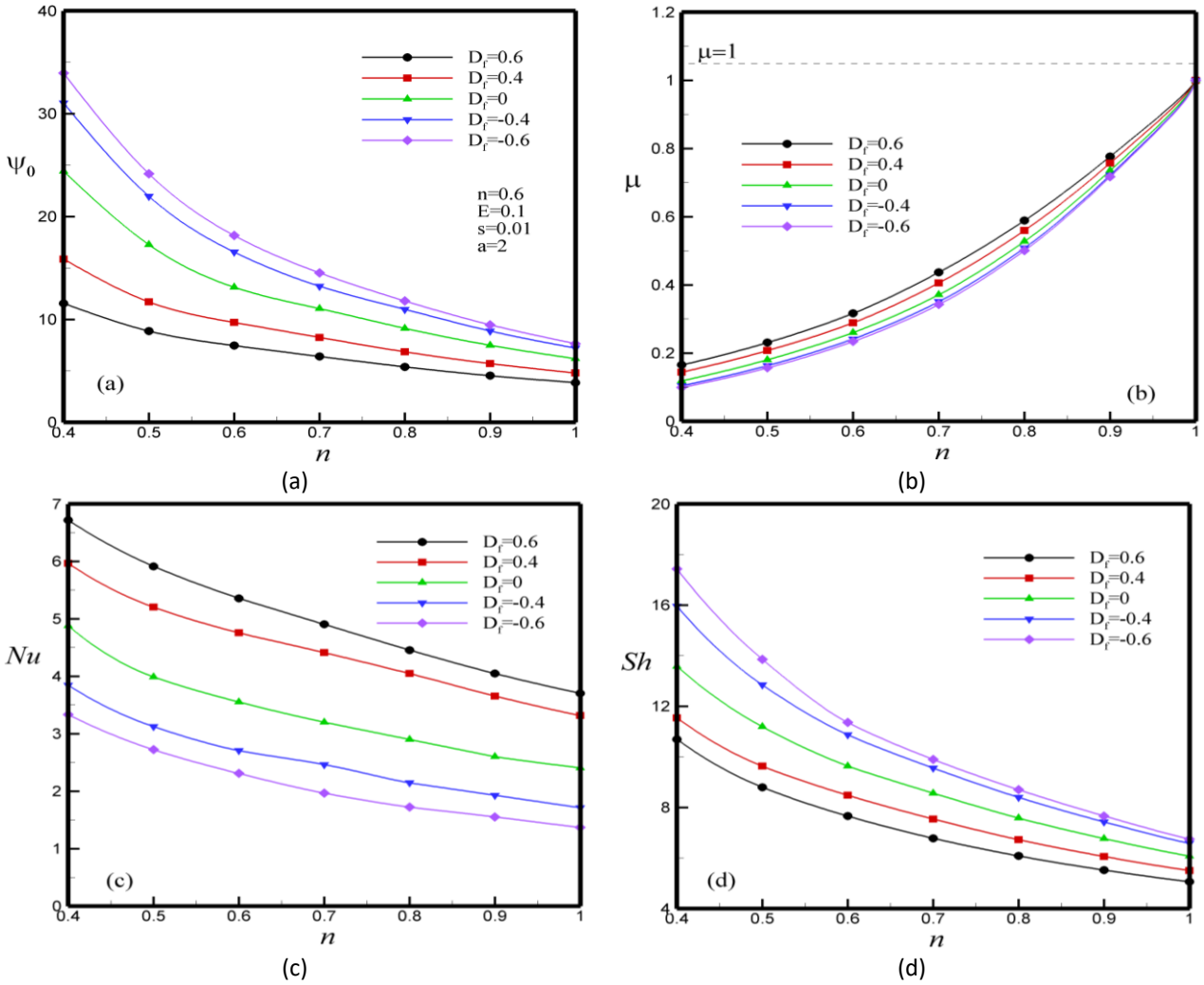

Fig. 14. Impact of D_f and n, on: (a) stream function, ψ_0; (b) apparent viscosity, μ; (c) Nu; (d) Sh, for $Ra_T = 10^4$, $Le = 10$, $N = -0.5$, $\gamma = 0°$ and $S_r = 0$.

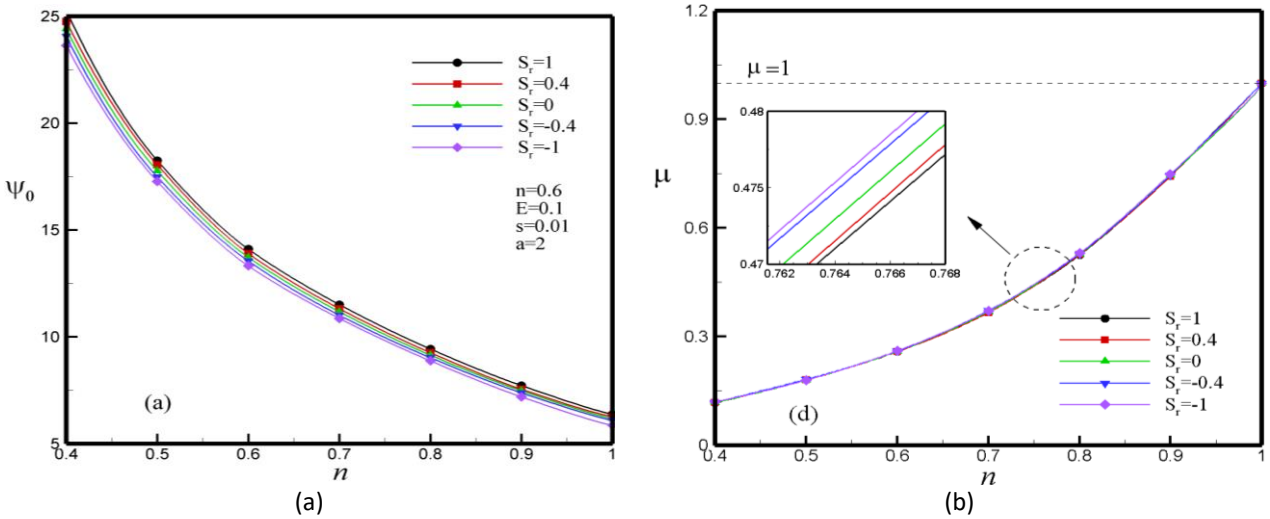

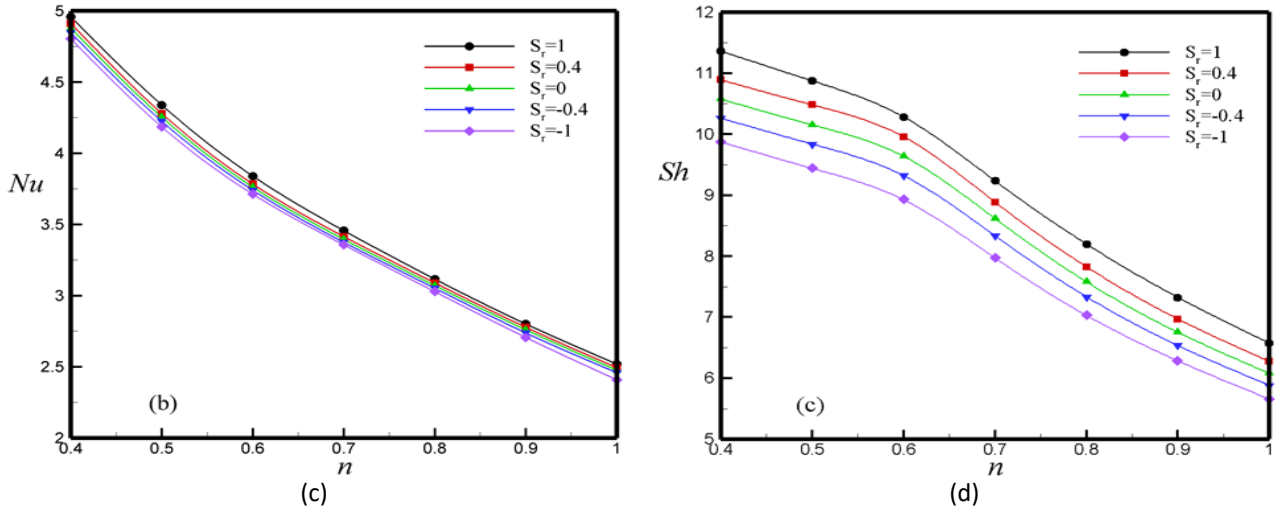

(c) (d)

Fig. 15. Effect of Soret number, S_r, and n, on: (a) ψ_0; (b) μ; (c) Nu; (d) Sh, for $Ra_T = 10^4$, $Le = 10$, $N = -0.5$, $\gamma = 0°$ and $D_f = 0$.

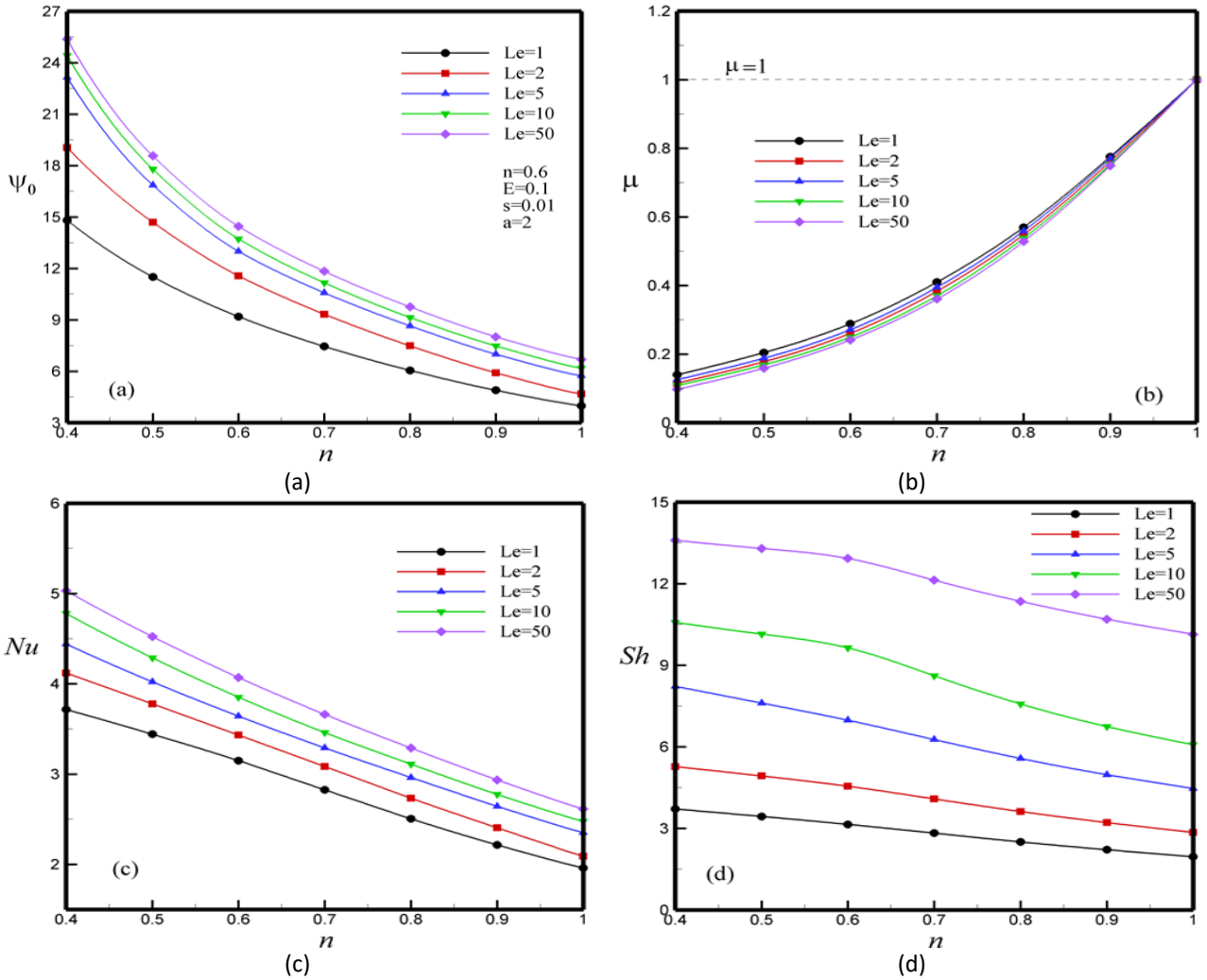

(a) (b)

(c) (d)

Fig. 16. Effect of Le and n on: (a) ψ_0; (b) apparent viscosity; μ, (c) Nu; (d) Sh, for $Ra_T = 10^4$, $N = -0.5$, $\gamma = 0°$ and $S_r = D_f = 0$.

Figures 16(c) and (d) show the variation of *Nu* and *Sh* vs. *n*. Indeed, the increasing *Le* causes a consdierable rise in Nu and Sh. As a result, the pattern confirms that thermal and mass exchange is

improved with the rise of *Le*, for various n. The convection intensity is lower for Newtonian fluids and in contrast to psuodoplastic fluids.

The impact of bouyancy ratio, N, on the stream function, apparent viscosity, *Nu* and *Sh* is given in Figure 17 for $Ra_T = 10^4$, $Le = 10$, $\gamma = 0°$ and $S_r = D_f = 0$. As N increases, the stream function is increased. In addition, with increase *n*, the stream function is small for Newtonian fluids and it increases for large values of n in shear-thinning fluids. Figure 17(b) illustrates the influence of N on apparent viscosity, where a slight variation in the apparent viscosity is remarked vs. N. The apparent viscocity $\mu = 1$ for Newtonian fluids, then it decreases rapidly to constant values for shear-thinning fluids $n = 0.4$. Figures. 17(c) and (d) show that *Nu* and *Sh* increase with N. When n decreases from 1 to 0.4, *Nu* and *Sh* tend towards an asymptotic value wich is a function of N from -1 to 1. This is due to the increase of the volume forces in the momentun equation. Morevere, the augementation of buoyancy ratio enhances the thermal and mass exchange. The mass exchange reaches a maximun asymptotic value faster than the thermal exchange. This is a direct consequence of the Lewis number ($Le = 10$) in the mass exchange. As n decreases from Newtonian fluids ($n = 1$) to shear-thinning fluids ($n = 0.4$), the thermal and mass exchange increase for all valeus of N.

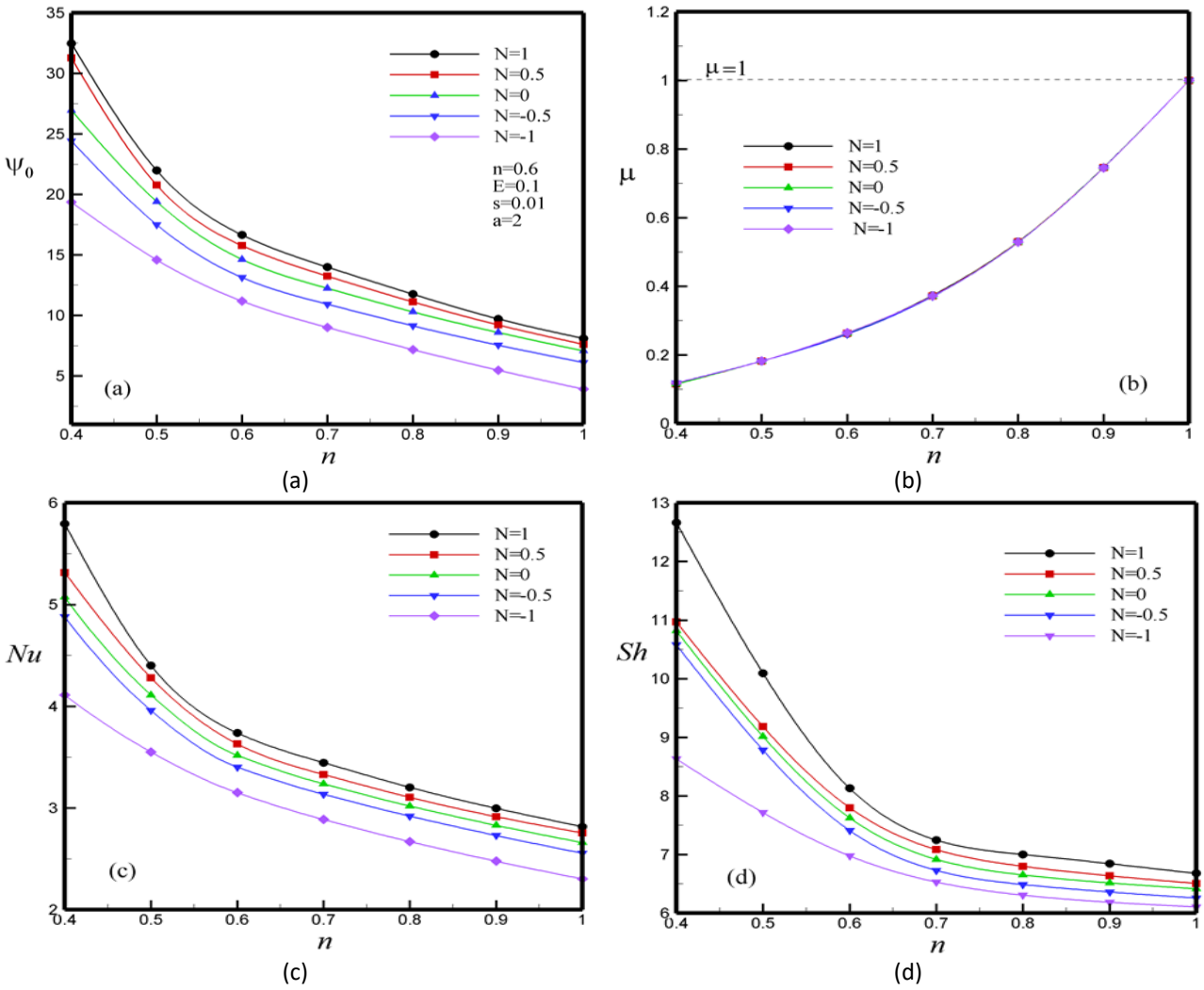

Fig. 17. Effect of bouyancy ratio, N, on: (a) ψ_0; (b) apparent viscosity, μ; (c) Nu; (d) Sh, for $Ra_T = 10^4$, $Le = 10$, $\gamma = 0°$ and $S_r = D_f = 0$.

The change of ψ_0, μ, Nu and Sh with the flow behavior index, n, for various cases of γ (0° to 90°) at $Ra_T = 10^4$, $Le = 10$ and $S_r = D_f = 0$ is shows in Figures 18(a)-(d). The results demonstrate that

the highest values of Nu, and Sh are found when $\gamma = 60°$. Decreasing the flow behavior index, n, enhances both the thermal and mass exchange. It clear from Figures 18(c) and (d) that for a given value of n, an increase in the inclination angle increases significantly both Nu and Sh. Figure 18(b) shows a decrease in viscosity with increased $\gamma°$. From Figures 18(c) and (d), it is proven that at $0.4 \leq n \leq 0.6$, *Nu* at $\gamma = 60°$ is more than that at $\gamma = 90°$. However, at $0.6 \leq n \leq 1$, *Nu* at $\gamma = 30°$ is more than that at $\gamma = 90°$. *Nu* increases significantly at $\gamma = 0°$. *Sh* augments with increasing γ from 0° to 90° and it is considrably enhanced.

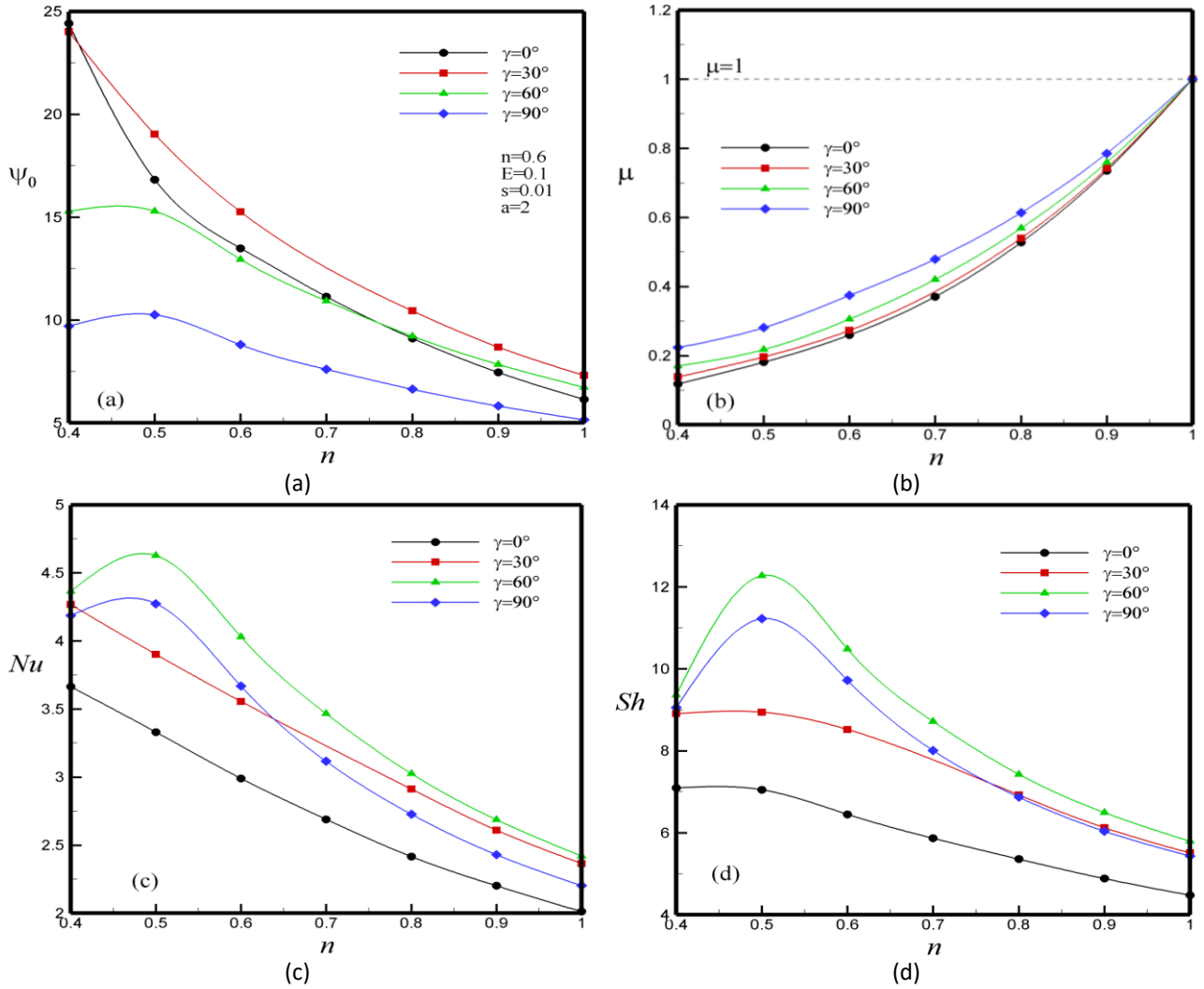

Fig. 18. Effect of inclined angel, γ, on: (a) ψ_0; (b) apparent viscosity, μ; (c) Nu; and (d) Sh, for $Ra_T = 10^4$, $Le = 10$ and $S_r = D_f = 0$.

5. Conclusions

The thermosolutal convection in an inclined cavity filled with non-Newtonian fluids was numerically examined. The effect of the Carreau-Yasuda rheological parameters, Rayliegh number, Ra_T ,Lewis number, Le, buoyancy ratio, N, Dufour and Soret numbers and inclination angle, γ, on the thermal and mass exchange was demonstrated. The main conclusion of the present investigation can be summarized as follows:

i. The thermal and mass exchange augments with decreasing s and a parameters and rising for the time constant parameter E, and a, and causes the apparent viscosity to drop slightly as the power-law index, n, decrease from Newtonian fluids to shear-thinning fluids.

ii. The decreased Ra_T improves both the thermal and mass exchange and apparent viscosity for different power-low index, n.
iii. The decrease n promotes the convection in the cavity and significantly increases the thermal and mass exchange. Thus, the decreases n favours the subercritical convection finit amplitude.
iv. The thermal exchange increases for rising Soret and Dufour parameters. The mass transfer is enhanced with increased *Sr* and D_f.
v. The apparent viscosity drops with increasing Soret and Dufour numbers.
vi. The increase in the Lewis number augments the thermal and mass exchange for various values of power-law index, n.
vii. The rise of buoyancy ratio increases considerably both the thermal and mass exchange. But the increase is not uniform for different power-low indices.
viii. The increase of buoyancy ratio yields a decrease in viscosity with decreased n.
ix. The maximum Nu and Sh increase with increased inclination angle for 60° to 90°, i.e., the convection process is enhanced at 60°.

Acknowledgement
Authors would like to thank Universiti Teknologi Malaysia for the funding from Takasago TTES R.K130000.7343.4B732.

References

[1] Beghein, C., F. Haghighat, and F. Allard. "Numerical study of double-diffusive natural convection in a square cavity." *International Journal of Heat and Mass Transfer* 35, no. 4 (1992): 833-846. https://doi.org/10.1016/0017-9310(92)90251-M
[2] Nield, D.A.; Bejan, A. "Convection in Porous Media." 2nd ed., Springer Verlag, New York, 1999.
[3] Benhadji, K., and P. Vasseur. "Double diffusive convection in a shallow porous cavity filled with a non-Newtonian fluid." *International communications in heat and mass transfer* 28, no. 6 (2001): 763-772. https://doi.org/10.1016/S0735-1933(01)00280-9
[4] Lamsaadi, M., M. Naimi, and M. Hasnaoui. "Natural convection of non-Newtonian power law fluids in a shallow horizontal rectangular cavity uniformly heated from below." *Heat and Mass Transfer* 41, no. 3 (2005): 239-249. https://doi.org/10.1007/s00231-004-0530-8
[5] Nield, D.A.; Bejan, A. "Convection in Porous Media, 4th ed., Springer-Verlag, 2013.
[6] Ingham, D.B.; Pop, I. "Transport Phenomena in Porous Media, Pergamon, 1998.
[7] Pop, I.; Ingham, D.B. "Convective Heat Transfer: Mathematical and Computational Modelling of Viscous Fluids and Porous Media." Pergamon, Oxford, 2001.
[8] Ohta, Mitsuhiro, Masayuki Ohta, Makoto Akiyoshi, and Eiji Obata. "A numerical study on natural convective heat transfer of pseudoplastic fluids in a square cavity." *Numerical Heat Transfer: Part A: Applications* 41, no. 4 (2002): 357-372. https://doi.org/10.1080/104077802317261218
[9] Kim, Gi Bin, Jae Min Hyun, and Ho Sang Kwak. "Transient buoyant convection of a power-law non-Newtonian fluid in an enclosure." *International journal of heat and mass transfer* 46, no. 19 (2003): 3605-3617. https://doi.org/10.1016/S0017-9310(03)00149-2
[10] Pericleous, K.A. "Heat transfer in differentially heated non-Newtonian cavities." *Int. J. Num. Methods Heat Fluid Flow* 1994, *4*(3), 229-248. https://doi.org/10.1108/EUM0000000004040
[11] Turan, O.; Sachdeva, A.; Chakraborty, N.; Poole, R.J. "Laminar natural convection of power-law fluids in a square enclosure with differentially heated walls subjected to constant temperatures." *J. Non-Newtonian Fluid Mech.* 2011, *166*, 1049-1063. https://doi.org/10.1016/j.jnnfm.2011.06.003
[12] Lamsaadi, M., M. Naimi, M. Hasnaoui, and M. Mamou. "Natural convection in a vertical rectangular cavity filled with a non-Newtonian power law fluid and subjected to a horizontal temperature gradient." *Numerical Heat Transfer, Part A: Applications* 49, no. 10 (2006): 969-990. https://doi.org/10.1080/10407780500324988
[13] Balmforth, Neil J., and Alison C. Rust. "Weakly nonlinear viscoplastic convection." *Journal of Non-Newtonian Fluid Mechanics* 158, no. 1-3 (2009): 36-45. https://doi.org/10.1016/j.jnnfm.2008.07.012

[14] Benouared, Ouahiba, Mahmoud Mamou, and Noureddine Ait Messaoudene. "Numerical nonlinear analysis of subcritical Rayleigh-Bénard convection in a horizontal confined enclosure filled with non-Newtonian fluids." *Physics of Fluids* 26, no. 7 (2014): 073101. https://doi.org/10.1063/1.4890829

[15] Alloui, Z., and P. Vasseur. "Natural convection of Carreau–Yasuda non-Newtonian fluids in a vertical cavity heated from the sides." *International Journal of Heat and Mass Transfer* 84 (2015): 912-924. https://doi.org/10.1016/j.ijheatmasstransfer.2015.01.092

[16] Kefayati, G.H.R. "Simulation of double diffusive natural convection and entropy generation of power-law fluids in an inclined porous cavity with Soret and Dufour effects (Part I: Study of fluid flow, heat and mass transfer)." *International Journal of Heat and Mass Transfer* 2016, *94*, 539-581. https://doi.org/10.1016/j.ijheatmasstransfer.2015.11.044

[17] Khechiba, Khaled, Mahmoud Mamou, Madjid Hachemi, Nassim Delenda, and Redha Rebhi. "Effect of Carreau-Yasuda rheological parameters on subcritical Lapwood convection in horizontal porous cavity saturated by shear-thinning fluid." *Physics of Fluids* 29, no. 6 (2017): 063101. https://doi.org/10.1063/1.4986794

[18] Krishna, M. Veera, and G. Subba Reddy. "MHD forced convective flow of non-Newtonian fluid through stumpy permeable porous medium." *Materials Today: Proceedings* 5, no. 1 (2018): 175-183. https://doi.org/10.1016/j.matpr.2017.11.069

[19] Wu, Ping-Yao, Ta-Jo Liu, and Hsu-Ming Chang. "Natural convection of non-Newtonian liquids in a cylindrical enclosure." *Numerical Heat Transfer* 25, no. 3 (1994): 363-371. https://doi.org/10.1080/10407789408955954

[20] Khellaf, K., and G. Lauriat. "Numerical study of heat transfer in a non-Newtonian Carreau-fluid between rotating concentric vertical cylinders." *Journal of non-newtonian fluid mechanics* 89, no. 1-2 (2000): 45-61. https://doi.org/10.1016/S0377-0257(99)00030-0

[21] Raisi, Afrasiab. "The influence of a pair constant temperature baffles on power-law fluids natural convection in a square enclosure." *Modares Mechanical Engineering* 15, no. 11 (2016): 215-224.

[22] Shahmardan, Mohammad Mohsen, Mahmood Norouzi, and Amir Naqhikhani. "Numerical Simulation of Non-Newtonian fluid flows through a channel with a cavity." *Modares Mechanical Engineering* 14, no. 6 (2014): 35-40.

[23] Guha, Abhijit, and Kaustav Pradhan. "Natural convection of non-Newtonian power-law fluids on a horizontal plate." *International Journal of Heat and Mass Transfer* 70 (2014): 930-938. https://doi.org/10.1016/j.ijheatmasstransfer.2013.11.001

[24] Kefayati, GH R. "Simulation of non-Newtonian molten polymer on natural convection in a sinusoidal heated cavity using FDLBM." *Journal of Molecular Liquids* 195 (2014): 165-174. https://doi.org/10.1016/j.molliq.2014.02.031

[25] Vinogradov, Igor, Lyes Khezzar, and D. Siginer. "Heat transfer of non-Newtonian dilatant power law fluids in square and rectangular cavities." *Journal of Applied Fluid Mechanics* 4, no. 3 (2011): 37-42.. https://doi.org/10.36884/jafm.4.03.11932

[26] Khelifa, N. Ben, Z. Alloui, H. Beji, and P. Vasseur. "Natural convection in a horizontal porous cavity filled with a non-Newtonian binary fluid of power-law type." *Journal of Non-Newtonian Fluid Mechanics* 169 (2012): 15-25. https://doi.org/10.1016/j.jnnfm.2011.11.002

[27] Kefayati, GH R., and H. Tang. "Three-dimensional Lattice Boltzmann simulation on thermosolutal convection and entropy generation of Carreau-Yasuda fluids." *International Journal of Heat and Mass Transfer* 131 (2019): 346-364. https://doi.org/10.1016/j.ijheatmasstransfer.2018.11.076

[28] Bihiche, K., M. Lamsaadi, and M. Hasnaoui. "Multiple steady state solutions for double-diffusive convection in a shallow horizontal rectangular cavity uniformly heated and salted from the side and filled with non-Newtonian power-law fluids." *Journal of Non-Newtonian Fluid Mechanics* 283 (2020): 104349. https://doi.org/10.1016/j.jnnfm.2020.104349

[29] Alloui, Z., R. Ouzani, and P. Vasseur. "Thermocapillary-buoyancy convection of a power-law fluid layer heated from below." *Journal of Non-Newtonian Fluid Mechanics* 282 (2020): 104332. https://doi.org/10.1016/j.jnnfm.2020.104332

[30] Tizakast, Youssef, Mourad Kaddiri, and Mohamed Lamsaadi. "Double-diffusive mixed convection in rectangular cavities filled with non-Newtonian fluids." *International Journal of Mechanical Sciences* 208 (2021): 106667. https://doi.org/10.1016/j.ijmecsci.2021.106667

[31] Rebhi, Redha, Mahmoud Mamou, and Noureddine Hadidi. "Bistability bifurcation phenomenon induced by non-Newtonian fluids rheology and thermosolutal convection in Rayleigh–Bénard convection." *Physics of Fluids* 33, no. 7 (2021): 073104. https://doi.org/10.1063/5.0051058

[32] Makayssi, T., M. Lamsaadi, and M. Kaddiri. "Natural double-diffusive convection for the Carreau shear-thinning fluid in a square cavity submitted to horizontal temperature and concentration gradients." *Journal of Non-Newtonian Fluid Mechanics* 297 (2021): 104649. https://doi.org/10.1016/j.jnnfm.2021.104649

[33] Gray, Donald D., and Aldo Giorgini. "The validity of the Boussinesq approximation for liquids and gases." *International Journal of Heat and Mass Transfer* 19, no. 5 (1976): 545-551. https://doi.org/10.1016/0017-9310(76)90168-X
[34] Yasuda, K. Y., R. C. Armstrong, and R. E. Cohen. "Shear flow properties of concentrated solutions of linear and star branched polystyrenes." *Rheologica Acta* 20, no. 2 (1981): 163-178. https://doi.org/10.1007/BF01513059
[35] Bird, B.R.; Armstrong, R.C.; Hassager, O. "Dynamic of polymeric liquids." John Wiley and Sons Inc., New York, 1978.
[36] Escudier, M. P., I. W. Gouldson, A. S. Pereira, F. T. Pinho, and R. J. Poole. "On the reproducibility of the rheology of shear-thinning liquids." *Journal of Non-Newtonian Fluid Mechanics* 97, no. 2-3 (2001): 99-124. https://doi.org/10.1016/S0377-0257(00)00178-6
[37] Allouche, Mohamed Hatem, Valéry Botton, Daniel Henry, Séverine Millet, R. Usha, and H. Ben Hadid. "Experimental determination of the viscosity at very low shear rate for shear thinning fluids by electrocapillarity." *Journal of Non-Newtonian Fluid Mechanics* 215 (2015): 60-69. https://doi.org/10.1016/j.jnnfm.2014.11.003
[38] Escudier, M. P., R. J. Poole, F. Presti, C. Dales, C. Nouar, C. Desaubry, L. Graham, and L. Pullum. "Observations of asymmetrical flow behaviour in transitional pipe flow of yield-stress and other shear-thinning liquids." *Journal of non-newtonian fluid mechanics* 127, no. 2-3 (2005): 143-155. https://doi.org/10.1016/j.jnnfm.2005.02.006
[39] Schneck, Paul, and George Veronis. "Comparison of some recent experimental and numerical results in Benard convection." *The Physics of Fluids* 10, no. 5 (1967): 927-930. https://doi.org/10.1063/1.1762243
[40] Plows, William H. "Some Numerical Results for Two-Dimensional Steady Laminar Bénard Convection." *The Physics of Fluids* 11, no. 8 (1968): 1593-1599. https://doi.org/10.1063/1.1692166